High resolution Fourier spectroscopy and laser spectroscopy of Cs2: The 21Σ+ g , (C) 21Π u , (D) 21Σ+ u , 31Σ+ g , and (E) 31Σ+ u electronic states

C. Amiot, W. Demtröder, and C. R. Vidal

Citation: The Journal of Chemical Physics **88**, 5265 (1988); doi: 10.1063/1.454755
View online: http://dx.doi.org/10.1063/1.454755
View Table of Contents: http://scitation.aip.org/content/aip/journal/jcp/88/9?ver=pdfcov
Published by the AIP Publishing

High resolution Fourier spectroscopy and laser spectroscopy of Cs_2: The $2\,^1\Sigma_g^+$, (C) $2\,^1\Pi_u$, (D) $2\,^1\Sigma_u^+$, $3\,^1\Sigma_g^+$, and (E) $3\,^1\Sigma_u^+$ electronic states

C. Amiot
Laboratoire Aimé Cotton,[a] *CNRS II, Bâtiment 505, Campus d'Orsay, 91405 Orsay Cédex, France*

W. Demtröder
Fachbereich Physik, Universität Kaiserslautern, D 6750, Kaiserslautern, West Germany

C. R. Vidal
Max Planck Institut für Extraterrestrische Physik, D 8046 Garching b. München, West Germany

(Received 29 September 1987; accepted 13 January 1988)

More than 8000 completely resolved rotational lines in the $E\,^1\Sigma_u^+ \rightarrow X\,^1\Sigma_g^+$, $E\,^1\Sigma_g^+ \rightarrow (2)\,^1\Sigma_g^+$, $E\,^1\Sigma_u^+ \rightarrow (1)\,^1\Pi_g$, $E\,^1\Sigma_u^+ \rightarrow (3)\,^1\Sigma_g^+$, $D\,^1\Sigma_u^+ \rightarrow (2)\,^1\Sigma_g^+$, $C\,^1\Sigma_u \rightarrow X\,^1\Sigma_g^+$, and $D\,^1\Sigma_u^+ \rightarrow X\,^1\Sigma_g^+$ transitions of Cs_2 have been accurately measured with the techniques of Fourier transform spectroscopy, Doppler-free polarization spectroscopy, and optical optical double resonance. The wave numbers of all these rotational lines were determined with an accuracy of 1 to 5×10^{-3} cm^{-1}. A thorough and simultaneous analysis of all the measured data yields molecular constants, potential energy curves, and dissociation energies for six different excited electronic states of the Cs_2 molecule.

I. INTRODUCTION

Spectroscopic information about the Cs_2 molecule has been proceeding rather slowly. The obvious reason is that the standard method using absorption spectroscopy has been restricted to relatively high temperatures ($\sim$550 K) where the vapor pressure of atomic cesium provides an appreciable concentration of Cs_2 molecules. This molecule is heavy, large, weakly bound, and the average rotational quantum number J is typically as large as 150 at these operating temperatures. In addition, vibrational levels up to $v = 15$ can be noticeably populated. Consequently, the ordinary absorption spectrum is rather congested.

Measurements of band spectra in the region 388–1050 nm, with a vibrational analysis of 218 bands in the 766.7 nm system, have been reported for the first time in the early work of Loomis and Kusch.[1] Similar to all other subsequent absorption studies, these authors could not resolve rotational lines, but they could determine vibrational constants from the position of the bandheads.

Later, Kusch and Hessel[2] reported a detailed vibrational analysis of the band system around 6250 Å. Also, Kusch and Hessel[3] refined and extended the earlier work by the use of both magnetic rotation and absorption spectra. The analysis of the 766.7 nm system could be extended to vibrational quantum numbers as high as $v'' = 100$ and $v' = 83$. From a partially resolved rotational structure they found the differences $B''-B'$ of the rotational constants in the lower and upper electronic states.

The Cs_2 absorption spectrum in the 480.0 nm region was measured by Lapp and Harris[4] and by Gupta *et al.*[5] It was analyzed through computer simulations by Tellinghuisen and Moeller.[6] These authors adjusted the shape of an, at that time unknown, upper potential energy curve until adequate agreement was obtained between the observed and the calculated absorption coefficients. Benedict *et al.*[7] used the same method to deduce the potential energy curves of the $A\,^1\Sigma_u^+$ and $a\,^3\Pi_u$ states: the absorption spectra in the wavelength range 800–1300 nm was measured over a wide temperature range. These absorption spectra in the same spectral region were previously observed by Bayley *et al.*[8] and Kostin and Khodovoi.[9] Later, Zouboulis *et al.*[10] have observed considerable absorption at wavelengths below 1.25 μm, extending up to 2.5 μm. It was believed that this new region of absorption was due to cesium dimers in the repulsive triplet state $(1)^3\Sigma_u^+ \rightarrow (1)^3\Sigma_g^+$ with possible contributions from higher polymers of cesium (Cs_3, Cs_4,...). Absolute cross-section measurements of Cs_2 in the spectral regions of 1100–3000 Å have been reported by Creek and Marr[11] while pronounced absorption bands were detected by Hotop and Niemax[12] in the wavelength region from 2300 to 3100 Å.

The development of commercial high power lasers has stimulated a growing interest in fluorescence spectroscopy of alkali-dimer molecules. Although this technique was first used with a high power tungsten halogen lamp as the optical pumping source byBenedict *et al.*,[13] only after using several lines of the argon laser and of the 632.8 nm helium–neon laser, McClintock and Balling[14] were able to observe atomic and molecular fluorescence. There has been considerable interest in the development of alkali dimer lasers, both as a tool for the spectroscopic study of the alkali molecules as well as a source of high-power quasitunable light. The latter aspect started with a paper by York and Gallagher.[15] The heavier alkalis, rubidium and cesium, are of particular interest since the density of energy levels approaches the point where almost continuous tuning might be achieved. Since equivalent transitions lie further to the red in the heavier molecules they offer the possibility of high power lasers in the near infrared where at present such sources are scarce and difficult to operate. However, so far most of the work has concentrated on the lighter alkalis such as lithium[16] and sodium.[17] Using

[a] Laboratoire associé à l'Université de Paris-Sud, Orsay, France.

 0021-9606/88/095265-17$02.10

different lines of an argon or krypton laser it has been possible to optically pump Li_2 lasers[18] and Na_2 lasers.[19–21] Laser induced fluorescence of Cs_2 excited by the Ar^+ laser lines have been studied byKato and Yoshihara.[22] A detailed analysis of the fluorescence was presented but without resolving the rotational structure of the observed bands. Höning *et al.*[23] reported on high resolution laser spectroscopy of the E–X band system. A combination of a supersonic molecular beam with laser-excited fluorescence allowed for the first time a complete resolution of rotational lines. Accurate molecular constants and the RKR potential energy curve of the $X\,^1\Sigma_g^+$ ground state up to $v'' = 72$ were derived. The $B\,^1\Pi_u \rightarrow X\,^1\Sigma_g^+$ transition near 627 nm was investigated by Kobyliansky *et al.*[24] and rotationally resolved by laser excitation spectroscopy with monochromatic detection of the fluorescence. Raab *et al.*[25] performed a thorough rotational analysis using Doppler-free polarization spectroscopy. Complete resolution of all rotational lines with rotational quantum numbers up to $J = 300$ and absolute wave number measurements with a traveling Michelson interferometer (lambdameter) to better than 0.001 cm^{-1} allowed a very accurate determination of the molecular constants of both the $X\,^1\Sigma_g^+$ ground state and the excited $B\,^1\Pi_u$ $v = 0$ vibrational level. Raab *et al.*[26] used molecular polarization spectroscopy with cw single mode tunable lasers as a Doppler-free technique to study also the Cs_2 $C\,^1\Pi_u \leftarrow X\,^1\Sigma_g^+$ system around 625 nm and several bands of the $D\,^1\Sigma_u^+ \leftarrow X\,^1\Sigma_g^+$ system. The optical–optical double-resonance technique (OODR) turned out to be very useful, allowing the unambiguous assignment even of perturbed transitions.

All previous studies considered fluorescence from an excited state of u symmetry down to the ground state $X\,^1\Sigma_g^+$. The possibility of observing infrared fluorescence to intermediate states of g symmetry was first pointed out by Bhaskar *et al.*[27] and Wu *et al.*[28] However, only the use of high resolution Fourier transform spectroscopy allowed the complete analysis of three intermediate states of g symmetry. The first $^1\Pi_g$ state was fully characterized by Amiot *et al.*[29,30] The first two excited $^1\Sigma_g^+$ states were also observed by the same authors[31] in other infrared spectral regions. Using a ring dye laser excitation near 17 000 cm^{-1}, Amiot and Verges[32] detected the first excited $^3\Sigma_g^+$ electronic state. However, the absolute vibrational assignment was not determined in that work.

With powerful lasers the study of ionization processes in Cs_2 became feasible. Collins *et al.*[33] investigated the multiphoton excitation of cesium through potentially resonant intermediate molecular states over the 620–500 nm spectral region with a tunable dye-laser source and a space-charge ionization detector. (It was found that a two-photon absorption could occur with high probability through a resonant intermediate state that was unstable against dissociation on the time scale of the multiphoton process.) Absolute probabilities for the absorption by Cs_2 via two-photon processes were investigated by Granneman *et al.*[34] These authors also reported values for the photoionization cross sections via the E intermediate state in the relevant two-step process.

Later, Collins *et al.*[35] used a pulsed, two-photon technique to study relative photolysis rates of the E, D, and C states of the Cs_2 molecule to the atomic $5D + 6S$ and $6P + 6S$ levels as a function of the excitation wavelength. This technique allowed determination of relative photolysis rates to each fine structure level.

Photolytic spectroscopy was employed by Collins *et al.*[36,37] to produce $5\,^2D$ and $6\,^2P$ atoms from the $X\,^1\Sigma_g^+$ state of Cs_2. The analysis of the photolysis spectrum led to the construction of approximate potential energy curves for two $^3\Sigma_u^+$ dissociative states correlating with the $6\,^2P$ and $6\,^2D$ atoms.

Two further studies were devoted to the decay mechanisms of the $E\,^1\Sigma_u^+$ state. Using the phase shift technique, Baumgartner *et al.*[38] made measurements of the lifetimes of levels pumped by various Ar^+ laser lines. Their extrapolation to zero pressure yielded the sum of the radiative and predissociation decay rates. The fact that different laser wavelengths resulted in different zero pressure extrapolations of τ led them to suggest that actually more than one state was excited by the different argon lines. The second study, reported by Wu *et al.*,[39] was devoted to the radiative decay, the predissociation to the $6S + 7S$, $6S + 5D$, and $6S + 6P$ atomic levels, and the excitation transfer collisions with ground state atoms and molecules. Absolute rates for the predissociation and the collisional excitation transfer out of the Cs_2 $E\,^1\Sigma_u^+$ state were reported. Preferential population of the magnetic sublevels of Cs ($6p\,^2P_{3/2}$) atoms produced by predissociation of the $C\,^1\Pi_u^+$ state along the repulsive molecular $b\,^3\Sigma_u^+$ state has been studied by Katô and Onomichi.[40] These authors observed the polarization of the atomic fluorescence $6p\,^2P^m_{3/2} \rightarrow 6s\,^2S_{1/2}$ between magnetic sublevels. By applying an external magnetic field they determined the population of the magnetic sublevels $6p\,^2P^m_{3/2}$ directly from the intensities of the fluorescence lines $6p\,^2P_{3/2} \rightarrow 6s\,^2S^{m\pm1}_{1/2}$ split due to the Zeeman effect.

The dissociation energy of the Cs_2 ground state has been controversial for some time and was resolved after the following studies. Using dye laser excitation of the $D\,^1\Sigma_u^+ \leftarrow X\,^1\Sigma_g^+$ system, Raab *et al.*[41] observed fluorescence progressions ranging from $v'' = 0$ to $v'' = 140$. Applying Le Roy's theory[42] they determined a value with an accuracy of ± 8 cm^{-1}. In order to overcome limitations in resolution, Weickenmeier *et al.*[43] applied the method of Doppler-free double-resonance polarization spectroscopy to high resolution measurements of rovibronic levels covering 99.5% of the dissociation energy. A long range analysis, based on 21 outer turning points of the potential energy curve and on calculated exchange energies and van der Waals coefficients C_n ($n = 6,8,10,12$) lead to a very accurate value for the dissociation energy $D_e = 3649.5 \pm 0.8$ cm^{-1}. During the course of this study, the hyperfine-induced mixing of high vibrational rotational levels of the Cs_2 $X\,^1\Sigma_g^+$ and $a\,^3\Sigma_u^+$ states was discovered. The observed spectral patterns were explained by u–g symmetry breaking induced by scalar nuclear–spin nuclear–spin interaction.[44]

The diatomic alkali molecules are attractive for quantum mechanical calculations since they may be considered as problems with two-valence electrons. In particular, the accurate knowledge of the potential energy curves, including the long range part near the dissociation limit, is of interest

for the quantitative understanding of atomic scattering problems, recombination processes, and line broadening phenomena. On the theoretical side, accurate *ab initio* calculations of potential energy curves are mainly available for the smaller diatomic molecules: Li_2, Na_2, K_2.

Two theoretical investigations of the ground state based on relativistic effective core potentials, were reported by Laskowski and Langhoff[45] and by Walch *et al.*[46] Jeung *et al.*[47] have developed a perturbative method to calculate the core–valence correlation energy and obtained good agreement with recent accurate FTS measurements. The long-range expansion coefficients C_n for the interactions $ns\,^2S + ns\,^2S$, $ns\,^2S + np\,^2P$ ($n = 3$ to 6) were calculated by Dalgarno,[48] Tang *et al.*,[49] and Vigne-Maeder.[50] Extrema in the long-range part of the potential energy curves were investigated previously by Movre and Pichler.[51] Quite recently Bussery and Aubert-Frecon[52] reported the results of an investigation of the long-range electrostatic, dispersion, and induced energy terms for the interactions between two identical alkali atoms. Calculations were initially performed neglecting spin–orbit effects and then including them. Very good agreement was obtained between calculated and experimental curves for the $X\,^1\Sigma_g^+$ state of Li_2 and for the $X\,^1\Sigma_g^+$, $(1)\,^1\Pi_g$ states of Na_2.

In previous FTS studies[29–31] the analysis was restricted to a fit of the vibrational and rotational differences for three electronic states: $(2)\,^1\Sigma_g^+$, $(1)\,^1\Pi_g$, and $(3)\,^1\Sigma_g^+$. In order to improve the self-consistency and the accuracy we chose to perform a global analysis incorporating all high resolution data involving the $(1)X\,^1\Sigma_g^+$, $(2)\,^1\Sigma_g^+$, $(3)\,^1\Sigma_g^+$, $(2)C\,^1\Pi_u$, $(2)D\,^1\Sigma_u^+$, $(1)\,^1\Pi_g$, and $E\,^1\Sigma_u^+$ electronic states.

The following spectroscopic techniques have been used for these measurements:

Fourier transform spectroscopy[29–31];

Doppler-free polarization spectroscopy and optical–optical double resonance[26];

Double resonance signals of the $D\,^1\Sigma_u^+ \rightarrow X\,^1\Sigma_g^+$ system[43];

Fabry–Perot spectroscopy of the fluorescence excited by laser light in a supersonic molecular beam.[23]

The experimental arrangements and methods used to obtain the Cs_2 spectra are described in Sec. II. Fluorescence spectra recorded by the different spectroscopic techniques are presented in Sec. III. The Sec. IV contains a description of the method of the global data analysis. The derived molecular constants, potential energy curves, dissociation energies, Λ-doubling constants are presented in Sec. V. The results and conclusions are summarized in Sec. VI.

II. EXPERIMENTAL

In this section the different experimental methods are briefly described.

(a) The first high resolution measurements were performed by Honing *et al.*[25] using the experimental arrangement shown in Fig. 1. The beam from a single mode argon ion laser crosses a molecular beam at right angles. The laser excited fluorescence is collected by the photomultipliers PM1 and PM2. The latter monitors the fluorescence behind a grating monochromator. A thorium hollow cathode lamp provides the reference wavelengths. The fluorescence wavelengths have been measured with a pressure scanned Fabry–Perot interferometer. About 450 fluorescence lines excited by the 476.5 and 488 nm Ar^+ laser lines were measured with an accuracy of 0.008 cm^{-1}.

(b) The subsequent high resolution laser spectroscopy of Cs_2 was Doppler-free polarization spectroscopy of the $C\,^1\Pi_u^+ \leftarrow X\,^1\Sigma_g^+$ and $D\,^1\Sigma_u^+ \leftarrow X\,^1\Sigma_g^+$ systems.[26] The schematic setup is shown in Fig. 2. The output of a single mode laser is split into a weak, linearly polarized probe beam and a stronger pump beam which is either circularly or linearly polarized. Both beams travel in opposite directions through the sample cell placed between two nearly crossed linear polarizers P1 and P2. A more detailed description of this technique can be found in Ref. 26 where the main advantages of molecular polarization spectroscopy are summarized: Doppler-free spectral resolution, high sensitivity, and the distinction between Q and P, R lines. Optical–optical double resonance (OODR) was used in conjunction with polarization spectroscopy.[26] The experimental setup is shown in Fig. 3. For "normal" polarization spectroscopy only dye laser 1 is used. The pump beam is chopped at the frequency f_1 and the polarization signal is detected by the photomultiplier denoted PM, followed by a lock-in amplifier LI. A relative wavelength calibration is achieved with a confocal Fabry–

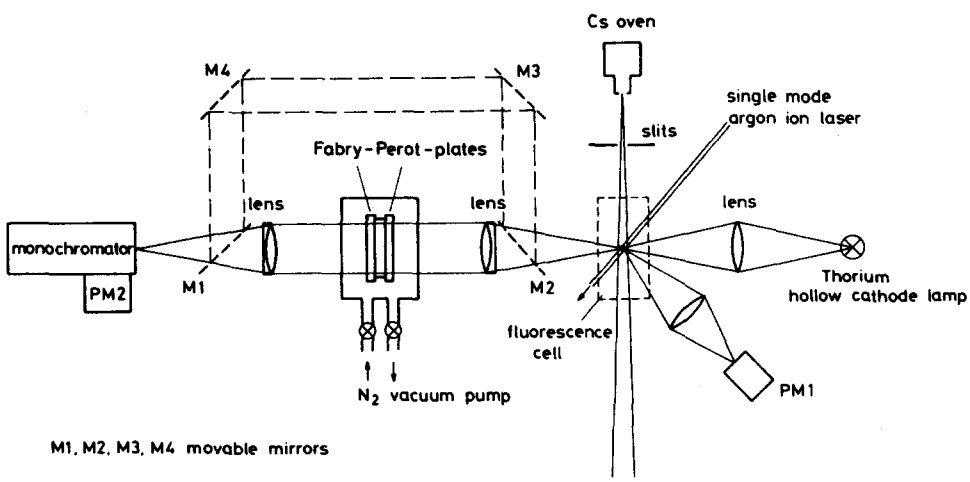

FIG. 1. Molecular beam fluorescence experiment. The beam from a single mode Ar^+ laser crosses the molecular beam from the Cs oven perpendicularly. The laser induced fluorescence is observed by the photomultipliers PM1 (total fluorescence) and PM2 placed after a grating monochromator. The line positions are measured by scanning a Fabry–Perot étalon. The wavelength calibration is done with thorium lines emitted from a hollow cathode lamp.

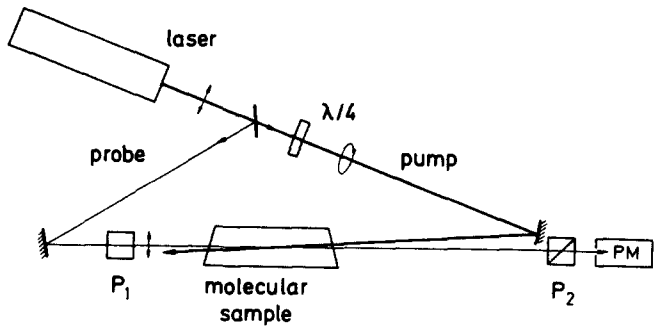

FIG. 2. Experimental arrangement for polarization spectroscopy. The output of a single mode dye laser is split into a weak linearly polarized probe beam and a stronger pump beam which is either circularly ($\lambda/4$ plate) or linearly polarized. The molecular sample is placed between two nearly crossed linear polarizers P1 and P2. After passing through the monisotropic sample, the detector PM receives a signal.

Perot interferometer FM which delivers frequency markers separated by 63 MHz. Absolute wavelength calibration is provided by comparing the dye laser wavelengths with a reference I_2 wavelength by means of a lambda meter. The $^{129}I_2$ reference line is the K hyperfine component of the $P(33)$ line in the 6←3 band.[53] More than 2000 lines in the $C\,^1\Pi_u \leftarrow C\,^1\Sigma_g^+$ and 200 lines in the $D\,^1\Sigma_u^+ \leftarrow X\,^1\Sigma_u^+$ system have been measured with an accuracy of 10^{-3} cm^{-1}.

(c) The third method used to obtain high resolution spectra is Fourier transform spectroscopy (FTS). Current interest in this technique arises from two basic properties demonstrated by Jacquinot[54] and P. Fellgett[55]: the multiplex advantage and the large transmission. The first theoretical and experimental results were obtained by Connes and Connes[56] at the Laboratoire Aimé Cotton. The main advantages of the interferometer used are its high resolution (2.5×10^{-3} cm^{-1}) and its scan speed (50 measurements per s). More details on the apparatus can be found in the thesis of Crepin.[57]

The experimental arrangement used to obtain the Cs_2 fluorescence spectra is shown in Fig. 4. The diatomic molecules have been generated in a heat pipe oven[58,59] made of stainless steel with a 97 μm mesh. The pipe was loaded with about 1.5 g of pure cesium and was operated with an argon pressure of typically 10 Torr and temperatures of about 600 K. The cesium pressure, at this temperature, is about 2.8 Torr,[60] which gives 4.6×10^{14} Cs_2 molecules per cm^3. These Cs_2 molecules in the heat-pipe oven were irradiated by the multimode laser lines of Ar^+ and Kr^+ ion laser (476.5, 488, 496.5, 501.7, 514.5, 647.1 nm) and of a cw dye laser (Rh 6G). Fluorescence in the backward direction is collected through a mirror with a hole towards the Fourier interferometer. When the ring dye laser is used, fluorescence in the forward direction is partially dispersed by a low resolution spectrometer and the resulting signal of the photomultiplier PMT is used to servo control the laser line to its intensity maximum. A Fabry–Perot FP controls the single mode operation of the laser, the wavelength of which is measured with a lambdameter (traveling Michelson interferometer).

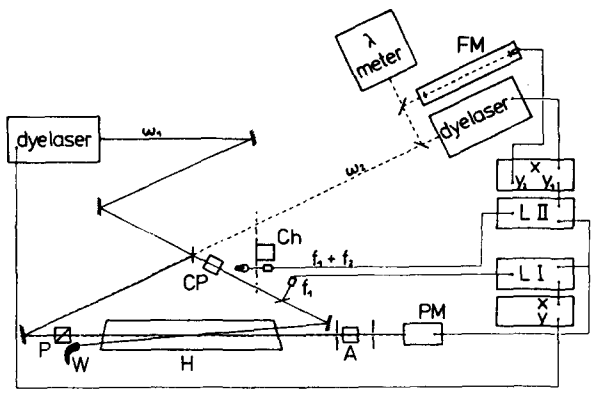

FIG. 3. Experimental arrangement for double-resonance polarization spectroscopy. The dyelaser with frequency ω_1 emits the pump beam at frequency ω_1. It is chopped at frequency f_1 by the chopper Ch. The probe beam, at ω_2, is collinearly superimposed to the pump beam but chopped at frequency f_2. Wavelengths calibration is done with the λ meter and the frequency marker Fabry–Perot interferometer FM. LI and LII are two lock-in amplifiers tuned to the frequencies f_1 and f_1+f_2, respectively. Polarization of the beam is done by the two linear polarizers P and A, and by the circular polarizer CP.

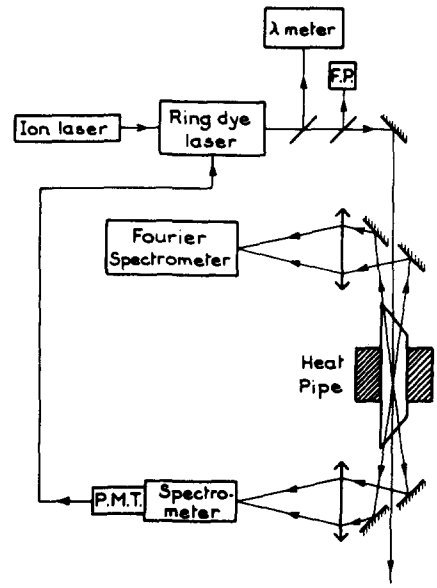

FIG. 4. Experimental setup for Fourier transform spectroscopy. The laser light comes either from a fixed frequency ion laser (Ar^+ or Kr^+), or from a ring dye laser. The wavelength of the emitted line is measured by a λ meter and single mode operation is monitored by a confocal Fabry–Perot FP. The backward laser induced fluorescence is sent towards the Fourier spectrometer. The emitted laser line is monitored with a low resolution spectrometer followed by a photomultiplier PMT.

III. OBSERVED SPECTRA

A schematic overview of all the observed transitions is given in Fig. 5. Basically three different electronic states were laser pumped: the $E\,^1\Sigma_u^+ + E'\,^1\Pi_u$ states, the $D\,^1\Sigma_u^+$, and the $C\,^1\Pi_u$ states. (The yet nonstudied $^1\Pi_u$ state is denoted E'.) Examples of spectra obtained with the spectroscopic methods denoted (a), (b), (c), in the previous section, will now be presented.

A. Excitation of the $E\,^1\Sigma_u^+ + E'\,^1\Pi_u$ states

It was achieved by using the lines of an argon ion laser. Höning *et al.*[25] used a collimated supersonic cesium beam to reduce the population densities in the higher vibrational ro-

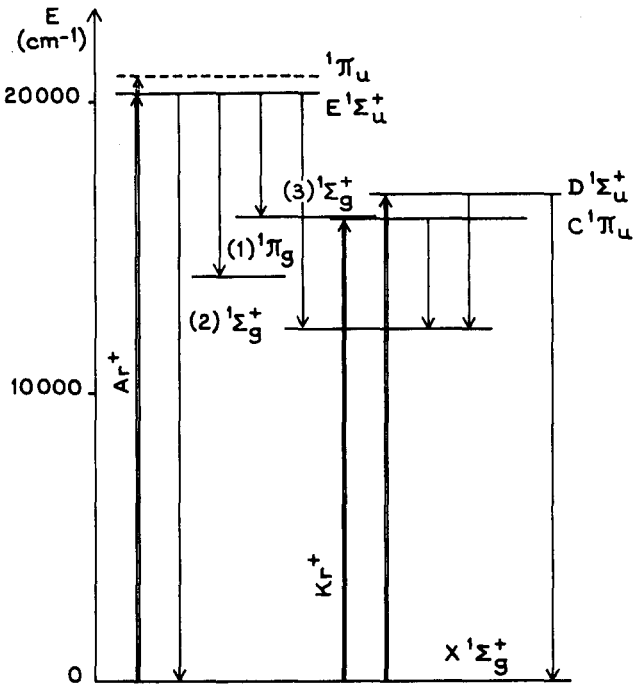

FIG. 5. Schematic representation of the excited electronic states and of the observed and analyzed fluorescence transitions.

tational levels of the ground state. Using a single mode laser stabilized to the center of a selected absorption line they obtain fluorescence progressions which consist of P and R lines as shown in Fig. 6. In order to obtain accurate molecular constants several fluorescence series, with P and R lines covering a large range of rotational quantum numbers J, had to be analyzed. In the supersonic beam, ground state levels with large J values are weakly populated. The molecular beam was then replaced by a sealed-off cell heated to about 500 K. Excitation by the single mode laser now results in a superposition of several fluorescence series. Figure 7 shows a section of the fluorescence spectrum excited in a cesium cell with a single mode argon laser set at 488 nm. Only nine levels of the upper state were observed, which were insufficient to provide the vibrational numbering. The results, however, were of so high quality that the molecular constants of the initial

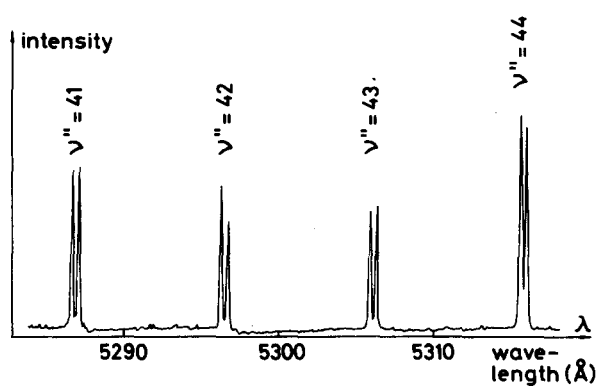

FIG. 6. Molecular beam fluorescence spectrum. Section of the fluorescence progression $E\,^1\Sigma_u^+$ $(v'=11, J'=45) \rightarrow X\,^1\Sigma_g^+$ $(v'', J''=44,46)$ after excitation by a single mode Ar^+ laser at 488 nm. The experimental arrangement of Fig. 1 is used.

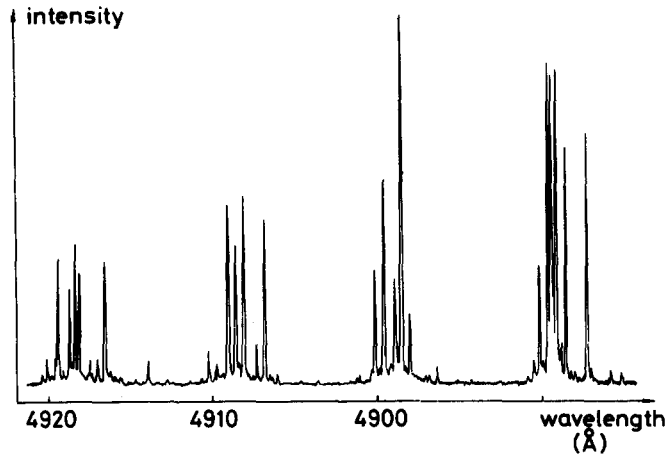

FIG. 7. Fluorescence spectrum excited in a cell containing Cs with a single mode Ar^+ laser at 488 nm. Same experimental arrangement as in Fig. 6.

state could be used for further assignments in the Fourier spectra.

Fluorescence which was excited in a heat pipe with a multimode Ar^+ laser was analyzed by high resolution Fourier spectroscopy.[29–31] In the visible region of the spectrum congested spectra like the one presented in Fig. 7, were observed. In addition, strong Q lines are present as clearly shown in the Fourier spectrum of Fig. 8. Höning *et al.*[23] have also noted that Q lines appear when the cesium heated in a cell was excited by the 488 nm laser line from higher vibrational levels of the ground state. The $E'\,^1\Pi_u$ state then lies above the $E\,^1\Sigma_u^+$ state. In Fourier spectra Q lines have been observed for the wavelengths 501.7, 496.5, 488, 476.5 nm. The great number of observed v', J' values has now allowed a vibrational assignment for the $E\,^1\Sigma_u^+$ state. It is worth noting that all the nine series obtained in single mode excitation could then be assigned with their vibrational quantum numbers. In the infrared spectral region three different fluorescence progressions were observed:

from 4100 to 4500 cm^{-1}: P,R doublets due to the transition $E\,^1\Sigma_u^+ \rightarrow (3)\,^1\Sigma_g^+$;

from 6100 to 6700 cm^{-1}: P,Q,R triplets due to the transition $E\,^1\Sigma_u^+ \rightarrow (1)\,^1\Pi_g$. An example of the Fourier spectrum is shown in Fig. 9. These spectra were only observed with the 514.5, 501.7, 496.5, and 488 nm laser lines;

from 7600 to 8400 cm^{-1}: P,R doublets are generated due to the $E\,^1\Sigma_u^+ \rightarrow (2)\,^1\Sigma_g^+$ transition. Q lines are observed up to 9300 cm^{-1} using the following laser lines: 476.5, 488, 496.5, and 501.7 nm.

B. Excitation of the $C\,^1\Pi_u$

More than 2000 lines in the $C\,^1\Pi_u \rightarrow X\,^1\Sigma_g^+$ band system have been accurately measured by Raab *et al.* using the technique of Doppler-free polarization spectroscopy. Figure 10 illustrates the different responses of the method to P, Q, and R lines, respectively. In the upper trace the pump polarization is linear and it is circular in the lower spectrum. While all three types of lines appear with linear polarization and with a Lorentzian shape, the Q lines show a dispersion shape with circular pump polarization and can therefore

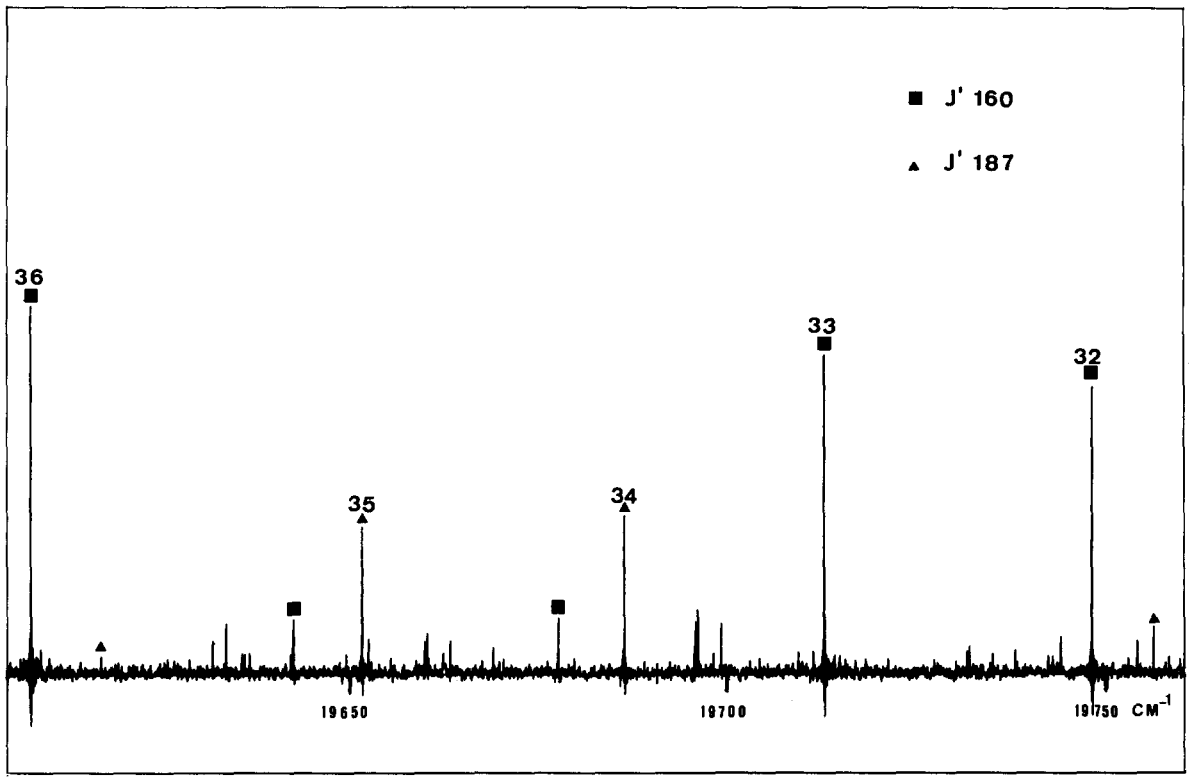

FIG. 8. Section of a Fourier spectrum after excitation of the Cs_2 molecules by the 465 nm Ar^+ laser line. The strongest progression is $^1\Pi_u$ $(v', J' = 160) \rightarrow X\,^1\Sigma_g^+$ $(v'', J'' = 160)$. The numbers above the Q lines give the v'' values. The pumped level is $v'' = 0, J'' = 160$ and the upper level is located at 21 301.84 cm^{-1}. The experimental setup of Fig. 4 is used.

easily be recognized. Double resonance experiments were then performed: Fig. 11 shows a normal polarization spectrum (lower trace) which was obtained by tuning the argon laser around 488 nm. The upper trace shows the double-resonance signals observed when a second dye laser is stabilized onto a selected transition and the single mode argon laser was tuned.

Fourier spectra, obtained after pumping Cs_2 molecules

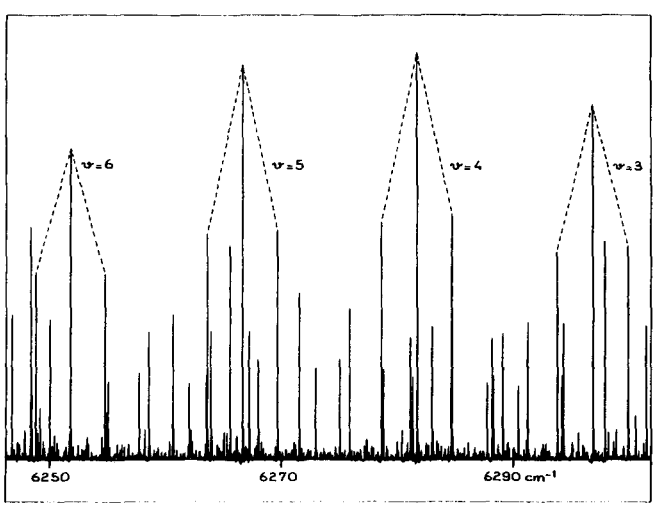

FIG. 9. Ar^+ (514.5 nm) laser induced fluorescence recorded by FTS in the infrared. Triplets of lines correspond to the transition $E\,^1\Sigma_u^+$ $(v' = 0, J' = 216) \rightarrow 1\,^1\Pi_g$ $(v'', J'' = 215,216,217)$. The experimental setup of Fig. 4 is used.

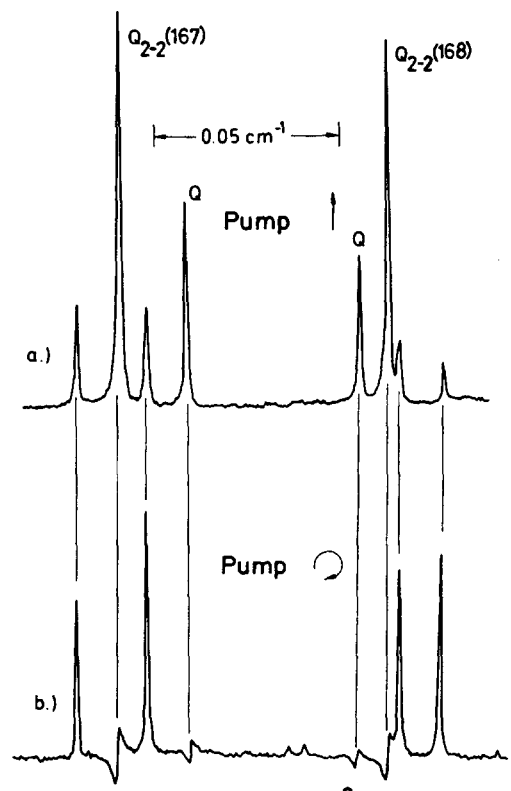

FIG. 10. Cs_2 polarization spectrum around $\lambda = 627.8$ nm. (a) Linearly polarized pump: strong Q lines; (b) circularly polarized pump: strong P and R lines. The experimental arrangement of Fig. 2 is used.

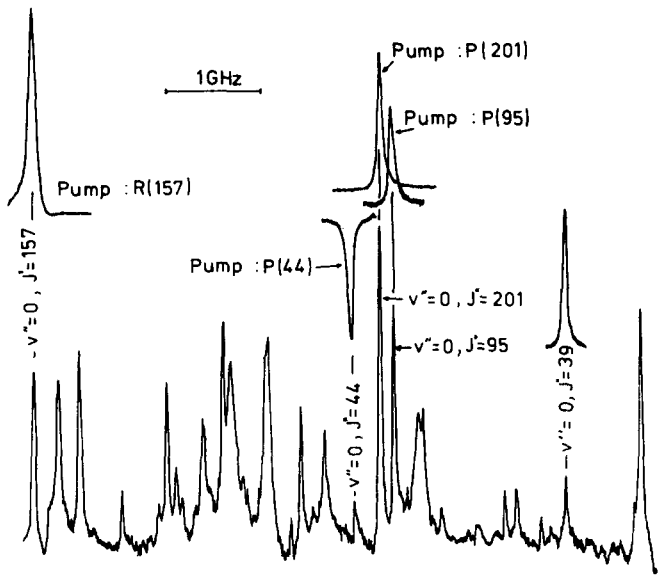

FIG. 11. Lower trace: normal polarization spectrum obtained with the Ar^+ laser tuned around 488 nm. Upper traces: the dye laser is stabilized onto a selected transition [for example, $R(157)$, $P(201)$...] while the second laser is tuned. The dye laser 1 in Fig. 3 is replaced by an Ar^+ laser.

with the 647.1 nm Kr^+ laser line, show doublets and isolated Q lines in the 400–4400 cm^{-1} region. This fluorescence is due to the $C\,^1\Pi_u \rightarrow (2)\,^1\Sigma_g^+$ transition. More intense line patterns were assigned by Amiot and Verges[31] to the $C\,^1\Pi_u(1u) \rightarrow (1)\,^3\Sigma_g^+(1g)$ transition.

C. Excitation of the $D\,^1\Sigma_u^+$ state

From double-resonance spectra, Raab *et al.*[41] have measured more than 40 vibrational progressions in the $D \leftarrow X$ system. Subsequently, Weickenmeier *et al.*[43] used Λ-type optical double resonance polarization spectroscopy to measure about 400 probed transitions. The lower vibrational levels covered the range from $v'' = 0$ to $v'' = 140$ and allowed an accurate determination of the ground state dissociation energy. New results were recently obtained giving accurate data down to $v' = 0$.[69]

Fourier spectroscopy was used to analyze the fluorescence spectra after excitation of the $D\,^1\Sigma_u^+$ state with a Rh 6G laser. A portion of the recorded spectrum after an excitation with the 570.4 nm laser line, is shown in Fig. 12. The doublet P, R lines in the $D\,^1\Sigma_u^+ \rightarrow (2)\,^1\Pi_g^+$ system are fully resolved. Rotational relaxation lines, with asymmetric intensity patterns, are well developed.

IV. ANALYSIS OF EXPERIMENTAL DATA AND MOLECULAR CONSTANTS

As described in the preceding section the wavelength of the 8090 lines have been determined and fitted simultaneously. Table I gives a summary of all the identified transitions and the spectroscopic methods that were used to obtain the data. The data of Refs. 23 and 26 have already been reduced simultaneously by Raab *et al.*[26] and gave accurate constants for the $X\,^1\Sigma_g^+$ and $C\,^1\Pi_u$ electronic states. The range of vibrational and rotational levels covered in our present final least-squares fit is shown in Figs.13 to 18 for the $E\,^1\Sigma_u^+$, $(3)\,^1\Sigma_g^+$, $(1)\,^1\Pi_g$, $C\,^1\Pi_u$, $D\,^1\Sigma_u^+$, $(2)\,^1\Sigma_g^+$ states, respectively. It is worth noting the increase of knowledge on the $E\,^1\Sigma_u^+$ state by using FTS and also the complementarity of all techniques to increase the data with respect to the $D\,^1\Sigma_u^+$ state.

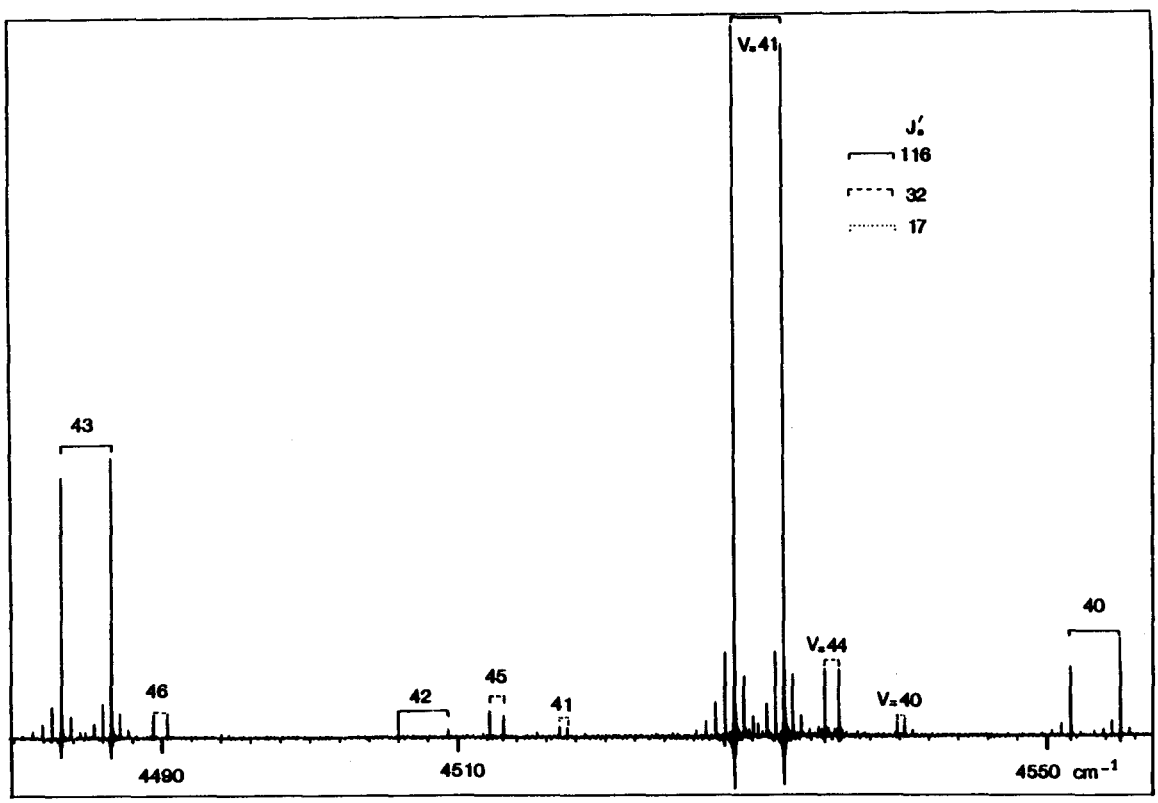

FIG. 12. Fourier spectrum of the $D\,^1\Sigma_u^+ \rightarrow (2)\,^1\Sigma_g^+$ infrared transition. The excitation is done with a dye laser at 570.4 nm. Upper levels with $J' = 17,32,116$ are excited. Rotational relaxations (nonsymmetric in intensity) are observed near the strongest doublet lines.

TABLE I. Summary of the Cs_2 spectroscopic data simultaneously reduced in this work.

Transition	Spectroscopic method	Ref.	Total number of measurements
$E\,^1\Sigma_u^+ \rightarrow X\,^1\Sigma_g^+$	single mode Ar^+ fluorescence molecular (FMB)	23	446
$E\,^1\Sigma_u^+ \rightarrow X\,^1\Sigma_g^+$	FTS	30	527
$E\,^1\Sigma_u^+ \rightarrow (3)\,^1\Sigma_g^+$	FTS	29	283
$E\,^1\Sigma_u^+ \rightarrow (1)\,^1\Pi_g$	FTS	30	1325
$E\,^1\Sigma_u^+ \rightarrow (2)\,^1\Sigma_g^+$	FTS	29	635
$C\,^1\Pi_u \rightarrow X\,^1\Sigma_g^+$	polarization spectroscopy (PS)	26	2180
$C\,^1\Pi_u \rightarrow X\,^1\Sigma_g^+$	V-type double resonance (VDR)	26	76
$D\,^1\Sigma_u^+ \rightarrow X\,^1\Sigma_g^+$	Λ-type double resonance (LDR)	43	668
$D\,^1\Sigma_u^+ \rightarrow (2)\,^1\Sigma_g^+$	FTS	31	1950

The identified lines of all transitions are described by the relation

$$\sigma = T'(v', J') - T''(v'', J'').$$

σ is the observed wave number, $T'(v', J')$ and $T''(v'', J'')$ are the term values of the upper and lower states, respectively, where for unperturbed systems the term value is given by

$$T(v, J) = \sum_{lk} (Y_{lk} + \delta y_{lk})(v + 1/2)^l \times [J(J+1) - \Lambda^2]^k.$$

The term δy_{lk} accounts for the Λ doubling of the $^1\Pi$ states

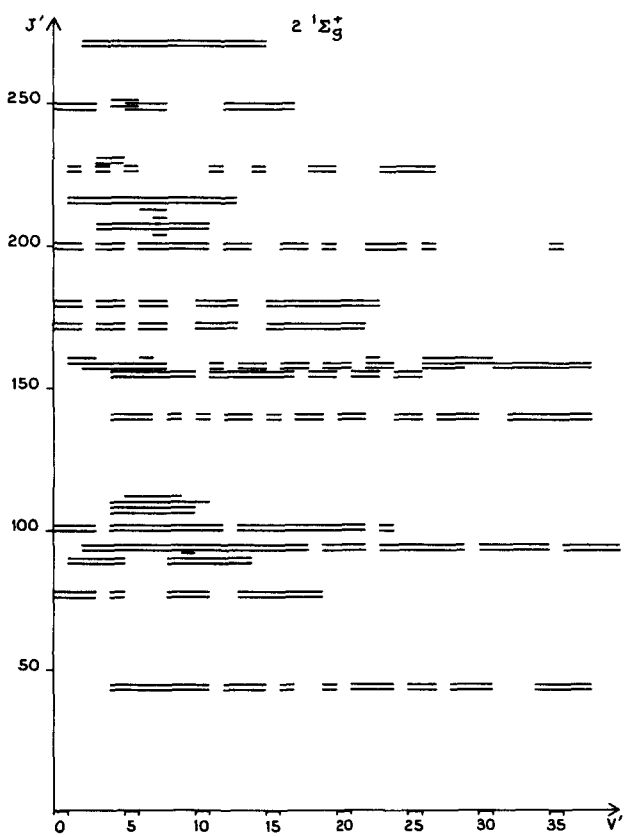

FIG. 13. Data fields of the $(2)\,^1\Sigma_g^+$ state levels. FTS measurements.

FIG. 14. Data fields of the $(1)\,^1\Pi_g$ state levels. FTS measurements.

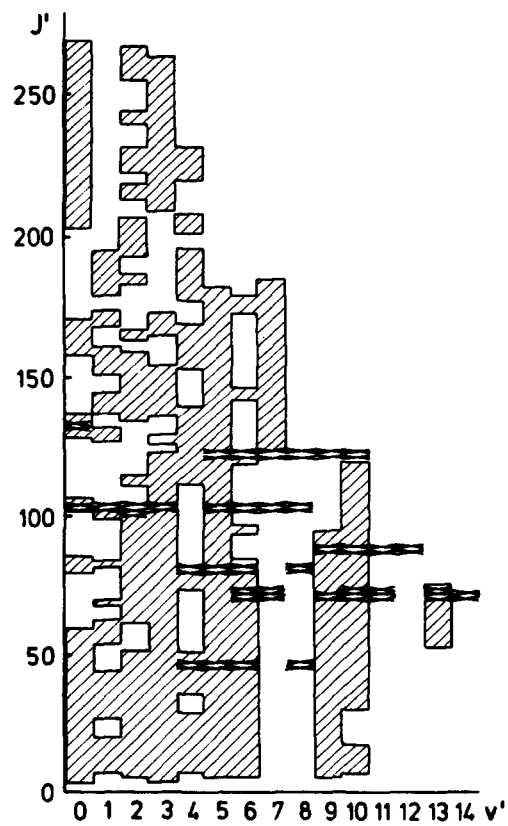

FIG. 15. Data field of the $C\,^1\Pi_u$ state. The dashed lines represent the data covered by double-resonance experiments. The crosses indicate LiF measurements.

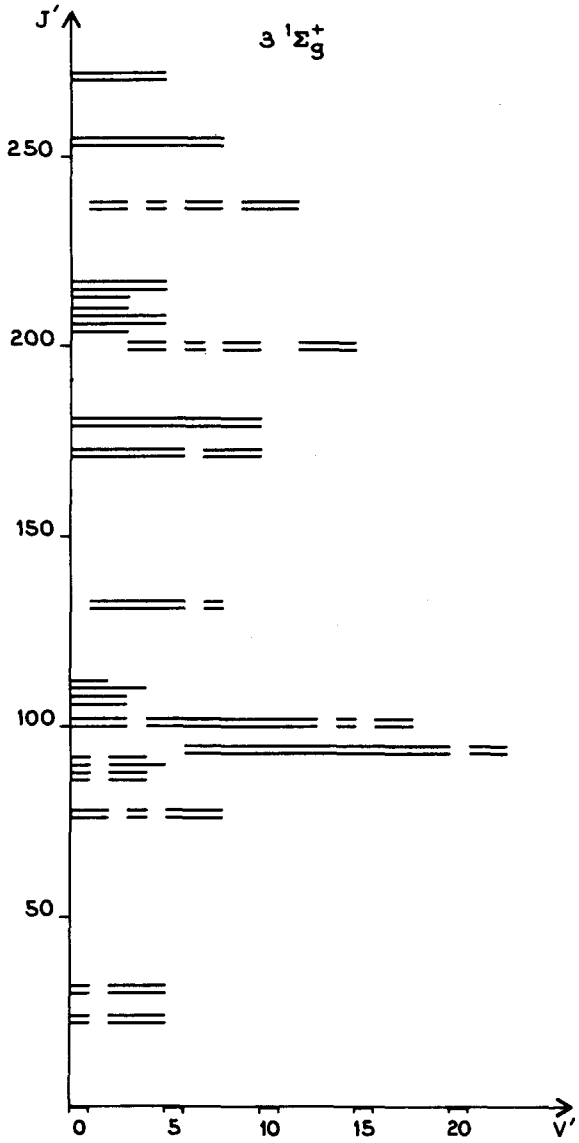

FIG. 16. Data field of the (3) $^1\Sigma_g^+$ state. FTS measurements.

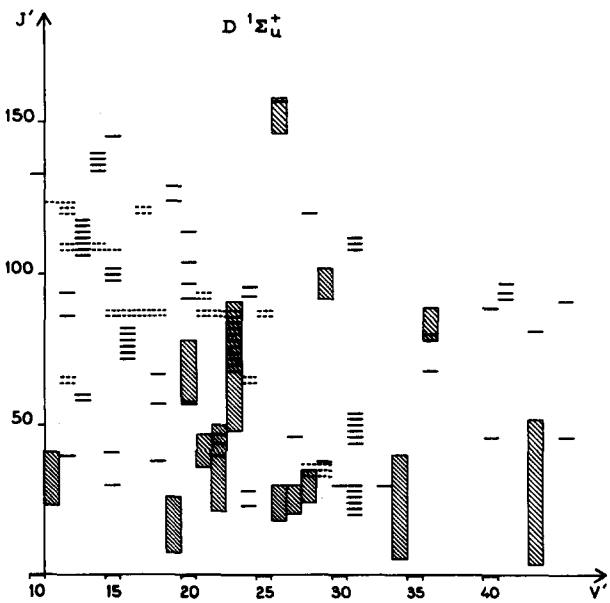

FIG. 17. Data field in the $D\,^1\Sigma_u^+$ state. Horizontal bars denote FTS measurements. All others are polarization and double-resonance measurements.

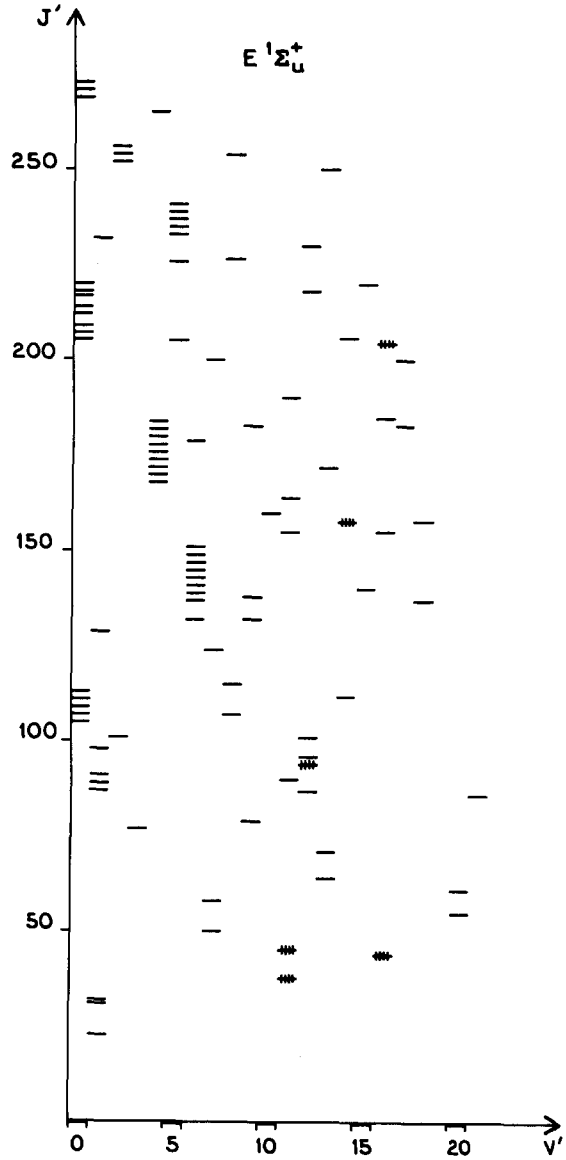

FIG. 18. Data field in the $E\,^1\Sigma_u^+$ state. Crossed bars are data given by for Raab *et al.* (Ref. 26). Other data are FTS measurements.

$[C\,^1\Pi_u$ and $(1)^1\Pi_g]$.[61] δ is 0 for the levels which give rise to the Q lines ($\Delta J = 0$) and $\delta = 1$ for the levels giving the P and R lines ($\Delta J = \mp 1$). The fitted constants Y_{lk} which are "Dunham-type" coefficients go over into genuine Dunham coefficients[62] only if the analysis is restricted to term values close to the potential minimum where a perturbation approach is valid. In our global fit we had to combine several sets of data which differed with respect to their accuracy. Such a situation requires a weighted least-squares fit[63] carried out in an iterative manner. At the end of the first fit we determined the rms errors for the different subsets of the measurements. The latter values were then used as a weighting factor for the subsequent least-squares fit. The method converges rapidly and the process is stopped typically after three iterations when the errors are determined within their own standard errors.

As shown by Raab *et al.*[26] several perturbed levels in the $C\,^1\Pi_u$ state had to be eliminated in order to obtain a meaningful set of Dunham-type coefficients.

TABLE II. Dunham-type coefficients for the $X\,^1\Sigma_g^+$ state of the Cs_2 molecule. All values are given in cm^{-1} together with their rms error.

		rms error	Relative rms error
$Y(1,0)$ =	4.201 945 529D + 01	5.22D − 05	1.2D − 06
$Y(2,0)$ =	− 8.191 119 659D − 02	7.81D − 06	9.5D − 05
$Y(3,0)$ =	− 8.956 147 856D − 05	4.43D − 07	4.9D − 03
$Y(4,0)$ =	− 3.778 821 382D − 07	1.08D − 08	2.8D − 02
$Y(5,0)$ =	− 4.997 048 889D − 09	9.04D − 11	1.8D − 02
$Y(0,1)$ =	1.174 389 283D − 02	3.22D − 07	2.7D − 05
$Y(1,1)$ =	− 2.214 617 666D − 05	8.66D − 09	3.9D − 04
$Y(2,1)$ =	− 9.086 593 791D − 08	5.77D − 10	6.3D − 03
$Y(3,1)$ =	− 3.187 120 048D − 10	1.32D − 11	4.1D − 02
$Y(4,1)$ =	− 6.071 747 475D − 12	1.14D − 13	1.8D − 02
$Y(0,2)$ =	− 3.776 488 731D − 09	1.76D − 11	4.6D − 03
$Y(1,2)$ =	− 1.401 351 101D − 11	5.49D − 13	3.9D − 02
$Y(2,2)$ =	− 9.703 017 103D − 14	1.70D − 14	1.7D − 01
$Y(3,2)$ =	− 3.172 406 079D − 15	1.35D − 16	4.2D − 02
$Y(0,3)$ =	3.739 114 037D − 15	3.59D − 16	9.6D − 02
$Y(1,3)$ =	− 2.066 314 208D − 16	1.46D − 17	7.1D − 02
$Y(2,3)$ =	3.514 346 423D − 18	3.98D − 19	1.1D − 01
$Y(0,4)$ =	− 2.047 925 717D − 20	2.39D − 21	1.1D − 01
$Y(1,4)$ =	1.664 965 766D − 21	1.16D − 22	7.0D − 02
$Y(2,4)$ =	− 3.153 923 352D − 23	3.20D − 24	1.0D − 01

The Dunham-type coefficients of the $X\,^1\Sigma_g^+$, $(2)\,^1\Sigma_g^+$, $D\,^1\Sigma_u^+$, $C\,^1\Pi_u$, $(1)\,^1\Pi_g$, $(3)\,^1\Sigma_g^+$, and $E\,^1\Sigma_u^+$ states which are obtained from the global least-squares fit of more than 8000 lines are listed in Tables II to VIII together with their rms errors. Besides the Dunham-type coefficients Table IX contains, for each subset of measurements defined in Table I, the rms error. The total standard error is equal to 4.8×10^{-3} cm^{-1}. We note that the polarization spectroscopy is almost three times more accurate than the other methods. FT spectroscopy compares very favorably with the other laser techniques.

The $D\,^1\Sigma_u^+$ electronic state is so strongly perturbed (by the $C\,^1\Pi_u$ and $^3\Pi$ states) that the Dunham coefficients sensitively depend on the experimental data set. This electronic state exhibits a strange vibrational spacing variation with v' as can be seen from Fig. 19. We chose to give in Table VII, not the unphysical fitting constants obtained in this work where only levels with $V'>11$ were introduced but rather, preliminary values obtained from a complete study includ-

TABLE III. Dunham-type coefficients for the $(2)\,^1\Sigma_g^+$ state of the Cs_2 molecule. All values are given in cm^{-1} together with their rms error.

		rms error	Relative rms error
$Y(0,0)$ =	1.211 406 703D + 04	1.69D − 03	1.3D − 07
$Y(1,0)$ =	2.335 173 654D + 01	4.32D − 04	1.8D − 05
$Y(2,0)$ =	7.069 190 709D − 03	5.25D − 05	7.4D − 03
$Y(3,0)$ =	− 2.520 232 918D − 04	2.96D − 06	1.1D − 02
$Y(4,0)$ =	1.222 171 303D − 06	8.27D − 08	6.7D − 02
$Y(5,0)$ =	− 6.204 570 966D − 09	1.11D − 09	1.7D − 01
$Y(6,0)$ =	1.117 699 294D − 11	5.80D − 12	5.1D − 01
$Y(0,1)$ =	7.459 006 779D − 03	3.84D − 07	5.1D − 05
$Y(1,1)$ =	1.871 578 023D − 07	2.58D − 08	1.3D − 01
$Y(2,1)$ =	− 1.220 432 954D − 07	2.08D − 09	1.7D − 02
$Y(3,1)$ =	1.643 914 568D − 09	9.07D − 11	5.5D − 02
$Y(4,1)$ =	− 1.776 319 179D − 11	1.97D − 12	1.1D − 01
$Y(5,1)$ =	8.554 112 912D − 14	1.68D − 14	1.9D − 01
$Y(0,2)$ =	− 3.087 331 432D − 09	1.85D − 11	6.0D − 03
$Y(1,2)$ =	4.102 394 330D − 12	4.85D − 13	1.1D − 01
$Y(2,2)$ =	− 1.006 963 569D − 13	1.77D − 14	1.7D − 01
$Y(3,2)$ =	− 1.328 535 478D − 15	3.31D − 16	2.4D − 01
$Y(0,3)$ =	3.365 908 804D − 15	3.42D − 16	1.0D − 01
$Y(1,3)$ =	− 2.072 610 838D − 17	3.03D − 18	1.4D − 01
$Y(0,4)$ =	− 7.097 087 374D − 21	2.08D − 21	2.9D − 01

TABLE IV. Dunham-type coefficients for the $(1)\,^1\Pi_g$ state of the Cs_2 molecule. All values are given in cm^{-1} together with their rms error. Only one Λ-doubling constant y_{01} is statistically significant.

		rms error	Relative rms error
$Y(0,0)$ =	1.391 342 250D + 04	1.65D − 03	1.1D − 07
$Y(1,0)$ =	1.843 934 630D + 01	7.38D − 04	4.0D − 05
$Y(2,0)$ =	− 1.017 051 613D − 01	1.46D − 04	1.4D − 03
$Y(3,0)$ =	3.687 551 189D − 04	1.23D − 05	3.3D − 02
$Y(4,0)$ =	4.634 826 006D − 06	4.59D − 07	9.9D − 02
$Y(5,0)$ =	− 1.396 304 445D − 07	6.28D − 09	4.5D − 02
$Y(0,1)$ =	7.815 352 442D − 03	3.64D − 07	4.6D − 05
$Y(1,1)$ =	− 4.979 090 151D − 05	4.60D − 08	9.2D − 04
$Y(2,1)$ =	5.997 151 015D − 08	7.91D − 09	1.3D − 01
$Y(3,1)$ =	2.147 184 113D − 09	5.73D − 10	2.6D − 01
$Y(4,1)$ =	− 7.385 494 093D − 11	1.88D − 11	2.5D − 01
$Y(5,1)$ =	3.336 122 294D − 12	2.43D − 13	7.2D − 02
$Y(0,2)$ =	− 5.655 645 303D − 09	1.73D − 11	3.0D − 03
$Y(1,2)$ =	− 4.872 624 169D − 11	6.49D − 13	1.3D − 02
$Y(2,2)$ =	5.815 394 109D − 14	9.13D − 14	1.5D + 00
$Y(3,2)$ =	8.720 009 043D − 14	5.00D − 15	5.7D − 02
$Y(4,2)$ =	− 2.886 140 530D − 15	8.80D − 17	3.0D − 02
$Y(0,3)$ =	− 1.263 940 216D − 15	3.16D − 16	2.5D − 01
$Y(1,3)$ =	1.079 041 267D − 16	2.59D − 18	2.4D − 02
$Y(0,4)$ =	− 1.250 070 698D − 20	1.91D − 21	1.5D − 01
$y(0,1)$ =	2.108 097 152D − 07	5.98D − 09	2.8D − 02

TABLE V. Dunham-type coefficients for the $C\,^1\Pi_u$ state of the Cs_2 molecule. All values are given in cm^{-1} together with their rms error. Three Λ-doubling constants Y_{01}, Y_{11}, and Y_{02} are required for the data.

		rms error	Relative rms error
$Y(0,0)$ =	1.594 869 084D + 04	2.34D − 04	1.4D − 08
$Y(1,0)$ =	2.966 458 013D + 01	4.79D − 04	1.6D − 05
$Y(2,0)$ =	− 4.214 620 174D − 02	2.74D − 04	6.5D − 03
$Y(3,0)$ =	− 5.374 399 612D − 04	6.19D − 05	1.1D − 01
$Y(4,0)$ =	− 1.147 279 538D − 05	6.08D − 06	5.3D − 01
$Y(5,0)$ =	− 1.447 573 360D − 06	2.19D − 07	1.5D − 01
$Y(0,1)$ =	1.236 068 642D − 02	3.26D − 07	2.6D − 05
$Y(1,1)$ =	− 6.688 828 231D − 05	9.97D − 08	1.4D − 03
$Y(2,1)$ =	9.815 249 723D − 07	5.60D − 08	5.7D − 02
$Y(3,1)$ =	− 1.646 503 509D − 07	1.28D − 08	7.8D − 02
$Y(4,1)$ =	1.633 103 341D − 08	1.30D − 09	7.9D − 02
$Y(5,1)$ =	− 6.390 778 940D − 10	4.85D − 11	7.5D − 02
$Y(0,2)$ =	− 8.722 038 958D − 09	1.75D − 11	2.0D − 03
$Y(1,2)$ =	1.965 593 780D − 10	3.35D − 12	1.7D − 02
$Y(2,2)$ =	− 1.897 404 959D − 11	1.76D − 12	9.3D − 02
$Y(3,2)$ =	1.518 362 895D − 12	3.82D − 13	2.5D − 01
$Y(4,2)$ =	6.951 308 792D − 14	3.86D − 14	5.5D − 01
$Y(5,2)$ =	− 1.390 152 717D − 14	1.51D − 15	1.0D − 01
$Y(0,3)$ =	2.530 000 548D − 15	3.50D − 16	1.3D − 01
$Y(1,3)$ =	− 6.398 073 738D − 16	2.13D − 17	3.3D − 02
$Y(2,3)$ =	1.111 276 315D − 16	7.85D − 18	7.0D − 02
$Y(3,3)$ =	− 1.282 483 733D − 17	7.95D − 19	6.2D − 02
$Y(0,4)$ =	− 1.023 811 850D − 20	2.31D − 21	2.2D − 01
$y(0,1)$ =	− 8.285 797 192D − 07	9.65D − 09	1.1D − 02
$y(1,1)$ =	− 2.009 976 941D − 08	1.17D − 09	5.8D − 02
$y(0,2)$ =	− 2.106 404 630D − 12	1.53D − 13	7.2D − 02

TABLE VI. Dunham-type coefficients for the (3) $^1\Sigma_g^+$ state of the Cs_2 molecule. All values are given in cm^{-1} together with their rms error.

		rms error	Relative rms error
$Y(0,0) =$	$1.597\,534\,672D+04$	$1.67D-03$	$1.0D-07$
$Y(1,0) =$	$2.242\,431\,398D+01$	$6.58D-04$	$2.9D-05$
$Y(2,0) =$	$-5.834\,544\,370D-02$	$1.29D-04$	$2.2D-03$
$Y(3,0) =$	$1.010\,008\,426D-03$	$1.03D-05$	$1.0D-02$
$Y(4,0) =$	$-1.821\,222\,320D-05$	$3.09D-07$	$1.6D-02$
$Y(0,1) =$	$8.230\,364\,301D-03$	$4.03D-07$	$4.8D-05$
$Y(1,1) =$	$2.028\,734\,060D-06$	$5.60D-08$	$2.7D-02$
$Y(2,1) =$	$-3.623\,779\,027D-07$	$7.38D-09$	$2.0D-02$
$Y(3,1) =$	$-1.369\,723\,599D-08$	$7.96D-10$	$5.8D-02$
$Y(4,1) =$	$2.496\,394\,746D-10$	$2.96D-11$	$1.1D-01$
$Y(0,2) =$	$-4.484\,397\,429D-09$	$1.94D-11$	$4.3D-03$
$Y(1,2) =$	$-8.415\,060\,472D-11$	$1.47D-12$	$1.7D-02$
$Y(2,2) =$	$1.901\,572\,399D-12$	$4.92D-14$	$2.5D-02$
$Y(0,3) =$	$5.626\,251\,153D-15$	$3.59D-16$	$6.3D-02$
$Y(1,3) =$	$-4.270\,651\,376D-17$	$1.19D-17$	$2.8D-01$
$Y(0,4) =$	$-1.163\,698\,424D-20$	$2.22D-21$	$1.9D-01$

TABLE VIII. Dunham-type coefficients for the $E\,^1\Sigma_u^+$ state of the Cs_2 molecule. All values are given in cm^{-1} together with their rms error.

		rms error	Relative rms error
$Y(0,0) =$	$2.019\,532\,147D+04$	$2.44D-03$	$1.2D-07$
$Y(1,0) =$	$2.898\,960\,508D+01$	$2.06D-03$	$7.1D-05$
$Y(2,0) =$	$-1.081\,931\,038D-01$	$8.05D-04$	$7.4D-03$
$Y(3,0) =$	$1.724\,256\,054D-03$	$1.49D-04$	$8.6D-02$
$Y(4,0) =$	$-3.895\,910\,460D-04$	$1.43D-05$	$3.6D-02$
$Y(5,0) =$	$2.102\,850\,238D-05$	$6.70D-07$	$3.1D-02$
$Y(6,0) =$	$-5.099\,646\,829D-07$	$1.21D-08$	$2.3D-02$
$Y(0,1) =$	$8.902\,237\,420D-03$	$4.17D-07$	$4.6D-05$
$Y(1,1) =$	$-2.768\,035\,619D-05$	$1.49D-07$	$5.3D-03$
$Y(2,1) =$	$-2.408\,594\,193D-07$	$4.17D-08$	$1.7D-01$
$Y(3,1) =$	$-8.747\,728\,818D-08$	$5.27D-09$	$6.0D-02$
$Y(4,1) =$	$8.270\,337\,174D-09$	$2.81D-10$	$3.4D-02$
$Y(5,1) =$	$-2.980\,052\,830D-10$	$5.35D-12$	$1.7D-02$
$Y(0,2) =$	$-3.418\,584\,882D-09$	$1.82D-11$	$5.3D-03$
$Y(1,2) =$	$-6.796\,291\,820D-11$	$2.87D-12$	$4.2D-02$
$Y(2,2) =$	$3.848\,620\,077D-12$	$4.54D-13$	$1.1D-01$
$Y(3,2) =$	$2.113\,825\,554D-13$	$4.38D-14$	$2.0D-01$
$Y(4,2) =$	$-4.142\,323\,297D-14$	$1.47D-15$	$3.5D-02$
$Y(0,3) =$	$1.982\,325\,275D-15$	$3.22D-16$	$1.6D-01$
$Y(1,3) =$	$2.049\,757\,211D-16$	$1.97D-17$	$9.6D-02$
$Y(2,3) =$	$-6.425\,591\,330D-17$	$1.63D-18$	$2.5D-02$
$Y(0,4) =$	$-1.354\,038\,932D-20$	$1.94D-21$	$1.4D-01$

ing levels with $V'=0$. Further details related to this electronic state will soon be published.[69]

V. MOLECULAR PROPERTIES

In this section we discuss the molecular properties such as the potential energy curves and the dissociation energies for each of the electronic states investigated.

A. Potential energy curves

Based on the Dunham-type coefficients of Tables II to VIII, we calculated the rotationless potentials using the "inverted perturbation approach" (IPA). This method was first proposed by Kosman and Hinze[64] and was further developed by Vidal and Scheingraber.[65] The method and its applications have recently been reviewed by Vidal.[66] The Rydberg–Klein–Rees[67] (RKR) potentials computed from the Dunham-type coefficients of Tables II to VIII, serve as a starting point for the variational method. In case of perturbed states it is important to calculate the potential energy curves with deperturbed constants.[68] In particular, for the two Π states, we have to consider the Λ doubling which originates from a perturbation due to neighboring electronic states belonging to the same complex. In calculating the potential energy curves we therefore have to use the constants associated with the unperturbed sublevels of the doublets. With these RKR potential energy curves the eigenfunctions ψ^0_{vJ} and eigenvalues E^0_{vJ} of the Schrödinger equation are calculated. If the zero order rotationless potential $U_0(R)$ is corrected by $\Delta U_0(R)$ the energies E^0_{vJ} are changed by the amount $\Delta E_{v,J}$ such that

$$\Delta E_{v,J} = \langle \psi^0_{vJ}(R) | \Delta U_0(R) | \psi^0_{vJ}(R) \rangle .$$

So far the potential energy change ΔU_0 has been described as a linear combination of the functions $f_i(R)$ which are products of Legendre polynomials and Gaussian functions[68] which dampen any unphysical oscillations of the potential energy curve:

TABLE VII. Dunham-type coefficients for the $D\,^1\Sigma_u^+$ state of the Cs_2 molecule. All values are given in cm^{-1} together with their rms error. These are preliminary constants (see Ref. 69 for more complete analysis).

		rms error	Relative rms error
$Y(0,0) = 1.669\,977$	$D+04$	$9D-02$	$5.3\,D-06$
$Y(1,0) = 1.928$	$D+01$	$5D-02$	$2.6\,D-03$
$Y(2,0) = 0.7$	$D-01$	$1D-02$	$0.14\,D00$
$Y(3,0) = -2.1$	$D-02$	$1D-03$	$4.8\,D-02$
$Y(4,0) = 13.2$	$D-04$	$7D-05$	$5.3\,D-02$
$Y(5,0) = -4$	$D-05$	$3D-06$	$7.5\,D-02$
$Y(0,1) = 7.87$	$D-03$	$3D-05$	$3.8\,D-03$
$Y(1,1) = -0.77$	$D-04$	$5D-06$	$6.5\,D-02$
$Y(2,1) = 0.23$	$D-05$	$3D-07$	$0.13\,D00$
$Y(3,1) = -3.8$	$D-08$	$7D-09$	$0.18\,D00$
$Y(4,1) = 0.17$	$D-09$	$6D-11$	$0.35\,D00$
$Y(0,2) = 0.341$	$D-08$	$7D-11$	$2.05\,D-02$

TABLE IX. rms error for each subset of measurements.

Transition	Ref.	Method	rms$\times 10^3$ (cm^{-1})
$E\,^1\Sigma_u^+ \rightarrow X\,^1\Sigma_g^+$	23	FMB[a]	8.7
$E\,^1\Sigma_u^+ \rightarrow X\,^1\Sigma_g^+$	30	FTS[b]	5.3
$E\,^1\Sigma_u^+ \rightarrow (3)\,^1\Sigma_g^+$	29	FTS	2.2
$E\,^1\Sigma_u^+ \rightarrow (1)\,^1\Sigma_g$	30	FTS	3.2
$E\,^1\Sigma_u^+ \rightarrow (2)\,^1\Pi_g^+$	29	FTS	2.1
$C\,^1\Sigma_u \rightarrow X\,^1\Sigma_g^+$	26	PS[c]	0.74
$C\,^1\Pi_u \rightarrow X\,^1\Sigma_g^+$		VDR[d]	1.9
$D\,^1\Sigma_u^+ \rightarrow X\,^1\Sigma_g^+$	43	LDR[e]	8.1
$D\,^1\Sigma_u^+ \rightarrow (2)\,^1\Sigma_g^+$	31	FTS	5.3

[a] FBM: fluorescence in molecular beam.
[b] FTS: Fourier transform spectroscopy.
[c] PS: polarization spectroscopy.
[d] VDR: V-type double-resonance spectroscopy.
[e] LDR: Λ-type double-resonance spectroscopy.

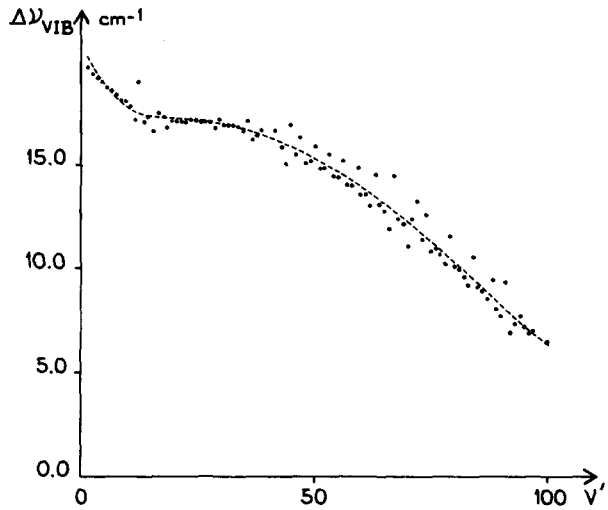

FIG. 19. Variation of the vibrational spacing $\Delta\nu_{vib} = G(v'+1) - G(v')$ with v' in the $D\,^1\Sigma_u^+$ state (Ref. 69).

$$\Delta U_0(R) = \sum_i c_i f_i(R).$$

The IPA potential will yield the measured eigenvalues E_{vJ}^{meas} if the c_i coefficients satisfy the condition

$$E_{vJ}^{meas} - E_{vJ}^{0} = \sum_i c_i \langle \psi_{vJ}^0(R) | f_i(R) | \psi_{vJ}^0(R) \rangle.$$

An iterative method is used to improve the agreement between the observed and the calculated energies. In order to limit the computational effort we selected a set of term values which are uniformly distributed over the data fields shown in Figs. 13 to 18. We used the following data fields $J(v_{min} - v_{max})$:

$E\,^1\Sigma_u^+$ state: 10(0–5), 40(0–15), 70(0–14), 106(0–12), 130(0–12), 158(1–13), 184(5–11), 205(0–11), 230(0–11),

$(3)^1\Pi_g^+$ state: 10(0–8), 40(0–8), 70(0–13), 106(0–14), 130(0–9), 158(0–12), 184(0–11),

$(1)^1\Pi_g$ state: 10(0–21), 40(0–22), 70(0–23), 105(0–24), 130(0–23), 158(0–21), 184(0–20), 205(0–19),

$(2)^1\Sigma_g^+$ state: 29(0–50), 45(0–50), 77(0–40), 93(0–50), 109(0–50), 139(0–35), 159(0–35), 179(0–20).

The $D\,^1\Sigma_u^+$ state is severely perturbed and only a RKR potential curve based on the preliminary molecular constants of Table VII is given.

Since Weichenmeier *et al.*[43] have calculated with great accuracy the IPA potential energy curve for the ground state $^1\Sigma_g^+$ up to the dissociation limit, we did not find it necessary to recalculate for this state a curve which is limited to lower vibrational quantum numbers. The same situation is true for the $C\,^1\Pi_u$ state, whose IPA curve was published previously by Raab *et al.*[26] Tables X to XIV list all the final outputs of the IPA method: the calculated vibrational term values $G(v)$, the turning points R_{min} and R_{max}, and the calculated rotational constant $B(v)$. (Table XIII gives RKR turning points for the $D\,^1\Sigma_u^+$ state.) The $G(v)$ values are defined as the energy eigenvalues of the rotationless molecule, the energy being counted from the minimum of the potential energy curve

$$G(v) = E_{v,J=0}.$$

The $B(v)$ values are the expectation values of $1/R^2$ for the rotationless molecule

TABLE X. The IPA potential energy curve of the Cs_2 (2) $^1\Sigma_g^+$ state.

v	$U(R)$	R_{min}	R_{max}	$B(v)*100$
0	11.6804	5.686 474 900	5.981 293 309	0.745 840 6
1	35.0445	5.582 368 092	6.092 828 567	0.745 837 4
2	58.4212	5.511 944 764	6.170 788 582	0.745 806 0
3	81.8090	5.455 485 074	6.234 883 300	0.745 749 6
4	105.2060	5.407 244 942	6.290 848 580	0.745 670 4
5	128.6109	5.364 591 182	6.341 310 841	0.745 570 5
6	152.0220	5.326 054 586	6.387 733 764	0.745 451 5
7	175.4379	5.290 715 770	6.431 032 262	0.745 314 6
8	198.8572	5.257 953 929	6.471 823 560	0.745 160 9
9	222.2787	5.227 326 422	6.510 547 461	0.744 991 2
10	245.7010	5.198 504 445	6.547 530 550	0.744 806 2
11	269.1229	5.171 235 804	6.583 023 304	0.744 606 3
12	292.5431	5.145 322 022	6.617 222 885	0.744 392 1
13	315.9605	5.120 603 547	6.650 287 849	0.744 163 7
14	339.3740	5.096 949 815	6.682 348 002	0.743 921 6
15	362.7823	5.074 252 346	6.713 511 242	0.743 665 9
16	386.1845	5.052 419 817	6.743 868 431	0.743 397 0
17	409.5792	5.031 374 457	6.773 496 949	0.743 115 0
18	432.9656	5.011 049 358	6.802 463 347	0.742 820 4
19	456.3425	4.991 386 435	6.830 825 354	0.742 513 2
20	479.7087	4.972 334 851	6.858 633 428	0.742 193 9
21	503.0634	4.953 849 787	6.885 931 974	0.741 862 7
22	526.4053	4.935 891 478	6.912 760 296	0.741 520 0
23	549.7334	4.918 424 430	6.939 153 378	0.741 166 1
24	573.0468	4.901 416 806	6.965 142 511	0.740 801 5
25	596.3443	4.884 839 921	6.990 755 806	0.740 426 4
26	619.6251	4.868 667 829	7.016 018 631	0.740 041 1
27	642.8880	4.852 876 990	7.040 953 972	0.739 646 1
28	666.1321	4.837 445 987	7.065 582 744	0.739 241 6
29	689.3564	4.822 355 295	7.089 924 052	0.738 827 7
30	712.5601	4.807 587 077	7.113 995 430	0.738 404 7
31	735.7421	4.793 125 009	7.137 813 041	0.737 972 7
32	758.9017	4.778 954 125	7.161 391 848	0.737 531 7
33	782.0378	4.765 060 666	7.184 745 773	0.737 081 6
34	805.1496	4.751 431 945	7.207 887 817	0.736 622 5
35	828.2363	4.738 056 211	7.230 830 173	0.736 154 3
36	851.2970	4.724 922 522	7.253 584 307	0.735 676 8
37	874.3308	4.712 020 620	7.276 161 016	0.735 190 2
38	897.3368	4.699 340 814	7.298 570 473	0.734 694 4
39	920.3143	4.686 873 889	7.320 822 246	0.734 189 7
40	943.2623	4.674 611 018	7.342 925 301	0.733 676 2
41	966.1800	4.662 543 715	7.364 888 004	0.733 154 5
42	989.0664	4.650 663 803	7.386 718 116	0.732 625 0
43	1011.9207	4.638 963 423	7.408 422 799	0.732 088 4
44	1034.7419	4.627 435 066	7.430 008 636	0.731 545 3
45	1057.5293	4.616 071 622	7.451 481 681	0.730 996 5
46	1080.2819	4.604 866 442	7.472 847 531	0.730 442 3
47	1102.9989	4.593 813 402	7.494 111 430	0.729 883 4
48	1125.6795	4.582 906 936	7.515 278 394	0.729 319 7
49	1148.3229	4.572 142 052	7.536 353 336	0.728 751 1

$R_e = 5.8318$ Å

TABLE XI. The IPA potential energy curve of the Cs_2 (1) $^1\Pi_g$ state.

v	$U(R)$	R_{min}	R_{max}	$B(v)*100$
0	9.1915	5.539 846 980	5.872 364 671	0.778 961 8
1	27.4275	5.433 822 100	6.012 408 039	0.774 011 8
2	45.4649	5.365 108 398	6.115 483 258	0.769 053 6
3	63.3052	5.311 659 526	6.203 591 059	0.764 101 0
4	80.9504	5.267 086 412	6.283 087 044	0.759 163 2
5	98.4027	5.228 475 698	6.356 861 715	0.754 245 9
6	115.6648	5.194 212 248	6.426 516 378	0.749 351 9
7	132.7391	5.163.293 266	6.493 047 408	0.744 481 9
8	149.6285	5.135 047 776	6.557 125 043	0.739 635 4
9	166.3357	5.109 001 888	6.619 226 171	0.734 811 2
10	182.8633	5.084 806 315	6.679 704 568	0.730 008 6
11	199.2136	5.062 193 812	6.738 830 866	0.725 227 8
12	215.3892	5.040 952 427	6.796 816 556	0.720 470 5
13	231.3921	5.020 907 956	6.853 829 038	0.715 740 4
14	247.2245	5.001 912 488	6.910 001 580	0.711 043 0
15	262.8883	4.983 837 588	6.965 440 472	0.706 385 2
16	278.3855	4.966 571 328	7.020 230 908	0.701 774 4
17	293.7180	4.950 018 222	7.074 442 470	0.697 217 3
18	308.8877	4.934 100 383	7.128 134 604	0.692 718 5
19	323.8964	4.918 757 423	7.181 361 812	0.688 279 9
20	338.7455	4.903 942 595	7.234 177 833	0.683 900 4
21	353.4362	4.889 614 813	7.286 637 804	0.679 576 6
22	367.9693	4.875 729 675	7.338 797 756	0.675 305 3
23	382.3451	4.862 234 484	7.390 711 503	0.671 085 1
24	396.5634	4.849 069 765	7.442 426 112	0.666 919 6
25	410.6240	4.836 174 810	7.493 977 910	0.662 818 3
26	424.5264	4.823 492 196	7.545 391 101	0.658 796 1
27	438.2702	4.810 968 328	7.596 680 019	0.654 871 0
28	451.8549	4.798 551 111	7.647 854 300	0.651 060 8
29	465.2798	4.786 187 581	7.698 924 790	0.647 379 4
30	478.5442	4.773 822 756	7.749 907 824	0.643 834 6
31	491.6470	4.761 399 219	7.800 826 838	0.640 426 9
32	504.5870	4.748 856 549	7.851 712 365	0.637 154 5
33	517.3643	4.736 129 818	7.902 604 191	0.634 037 0
34	529.9835	4.723 144 865	7.953 565 682	0.631 204 8
35	542.4657	4.709 809 138	8.004 732 799	0.629 116 8

$R_e = 5.6973$ Å

TABLE XII. The IPA potential energy curve of the Cs_2 (3) $^1\Sigma_g^+$ state.

v	$U(R)$	R_{min}	R_{max}	$B(v)*100$
0	11.1856	5.403 364 297	5.704 351 360	0.823 054 4
1	33.4970	5.296 282 350	5.818 927 505	0.823 196 4
2	55.6988	5.223 458 157	5.899 603 067	0.823 252 8
3	77.7978	5.164 859 545	5.966 446 611	0.823 211 8
4	99.7992	5.114 687 499	6.025 290 417	0.823 062 6
5	121.7075	5.070 292 113	6.078 803 027	0.822 798 2
6	143.5264	5.030 196 503	6.128 467 411	0.822 414 4
7	165.2594	4.993 488 054	6.175 206 289	0.821 907 4
8	186.9096	4.959 577 810	6.219 642 352	0.821 271 5
9	208.4802	4.928 062 332	6.262 227 357	0.820 502 7
10	229.9729	4.898 594 967	6.303 309 770	0.819 605 5
11	251.3873	4.870 802 234	6.343 160 754	0.818 599 2
12	272.7210	4.844 352 359	6.381 968 078	0.817 514 7
13	293.9717	4.819 127 755	6.419 826 377	0.816 378 1
14	315.1401	4.795 197 398	6.456 775 658	0.815 187 2
15	336.2317	4.772 551 279	6.492 899 363	0.813 897 2
16	357.2539	4.751 038 333	6.528 386 746	0.812 433 8
17	378.2113	4.730 511 535	6.563 464 509	0.810 734 8
18	399.1017	4.710 880 916	6.598 271 048	0.808 795 2
19	419.9173	4.692 085 274	6.632 834 192	0.806 674 3
20	440.6506	4.674 072 226	6.667 155 279	0.804 448 3

$R_e = 5.5518$ Å

TABLE XIII. The RKR potential energy curve of the Cs_2 $D\,^1\Sigma_u^+$ state.

v	$U(R)$	R_{min}	R_{max}	$B(v)*100$
0	9.722	5.5263	5.8515	0.7832
1	29.080	5.4306	5.9920	0.7759
2	48.424	5.3706	6.0955	0.7691
3	67.682	5.3245	6.1838	0.7627
4	86.803	5.2861	6.2632	0.7566
5	105.754	5.2525	6.3367	0.7510
10	197.641	5.1223	6.6513	0.7273
15	285.741	5.0241	6.9106	0.7097
20	372.231	4.9454	7.1303	0.6961
25	458.408	4.8799	7.3233	0.6843
30	544.196	4.8225	7.5030	0.6730
35	628.780	4.7708	7.6796	0.6605
40	711.543	4.7259	7.8574	0.6457

$R_e = 5.677$ Å

$$B(v) = \frac{\hbar}{4\pi c\mu}\left\langle \psi_{v,J=0}\left|\frac{1}{R^2}\right|\psi_{v,J=0}\right\rangle.$$

The potential energy curves are represented in Fig. 20.

It is worth noting that predissociation effects are important in the $(3)\,^1\Sigma_g^+$ state. The fluorescence series are limited and suddenly break off.

This effect is clearly shown by calculations of Franck–Condon factors (FCF) and by a comparison with the observed intensities. Figure 21 compares the observed intensities in the Fourier spectra and the calculated FCF for the transition $E\,^1\Sigma_u^+ \rightarrow (1)\,^1\Pi_g$ $(J' = 254, v' = 1 \rightarrow v'', J'' = 253)$. For the transition $E\,^1\Sigma_u^+ \rightarrow (3)\,^1\Sigma_g^+$ $(J' = 101, v' = 2 \rightarrow v'', J'' = 100)$ Fig. 22 clearly shows the strongly reduced measured intensities as compared with the calculated Franck–Condon factors.

The $D\,^1\Sigma_u^+$ electronic state is also strongly perturbed and many observed fluorescence series had to be omitted from the global least-squares fit.

TABLE XIV. The IPA potential energy curve of the Cs_2 $E\,^1\Sigma_u^+$ state.

v	$U(R)$	R_{min}	R_{max}	$B(v)*100$
0	14.4576	5.210 317 612	5.475 237 702	0.888 757 4
1	43.2355	5.121 730 268	5.582 057 839	0.885 846 7
2	71.8041	5.063 117 431	5.659 235 022	0.882 864 7
3	100.1578	5.016 868 778	5.724 446 160	0.879 790 6
4	128.2879	4.977 871 806	5.782 850 904	0.876 612 1
5	156.1834	4.943 785 732	5.836 825 145	0.873 320 9
6	183.8326	4.913 307 232	5.887 704 538	0.869 909 4
7	211.2233	4.885 627 511	5.936 338 129	0.866 366 8
8	238.3425	4.860 211 361	5.983 319 307	0.862 676 4
9	265.1762	4.836 688 193	6.029 100 332	0.858 814 2
10	291.7083	4.814 786 703	6.074 055 071	0.854 749 6
11	317.9193	4.794 290 582	6.118 513 458	0.850 446 6
12	343.7856	4.775 013 761	6.162 778 909	0.845 864 7
13	369.2794	4.756 799 710	6.207 141 019	0.840 955 6
14	394.3675	4.739 538 451	6.251 902 122	0.835 651 4
15	419.0099	4.723 177 266	6.297 430 735	0.829 846 0
16	443.1565	4.707 703 284	6.344 224 004	0.823 377 8
17	466.7433	4.693 109 892	6.392 939 076	0.816 037 2
18	489.6925	4.679 376 818	6.444 396 279	0.807 628 9

$R_e = 5.3382$ Å

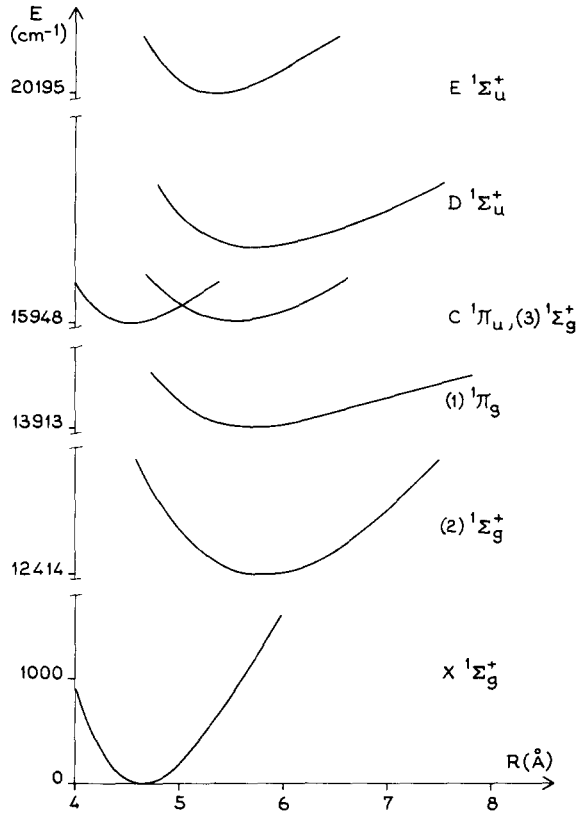

FIG. 20. Potential energy curves for the Cs_2 electronic states studied in the present paper. Only the studied range is shown.

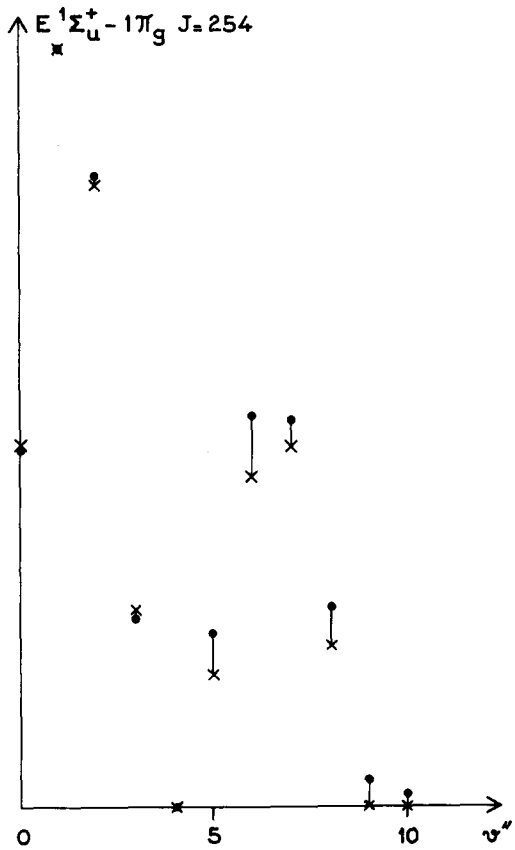

FIG. 21. Comparison between observed line intensities ($\times$) and calculated Franck–Condon factors (●) for the transitions $E\,^1\Sigma_u^+$ ($v' = 1, J' = 254$) $\rightarrow (1)\,^1\Pi_g$ ($v'', J'' = 235$). Normalization is such that the strongest observed and calculated intensities are equal ($v' = 1$).

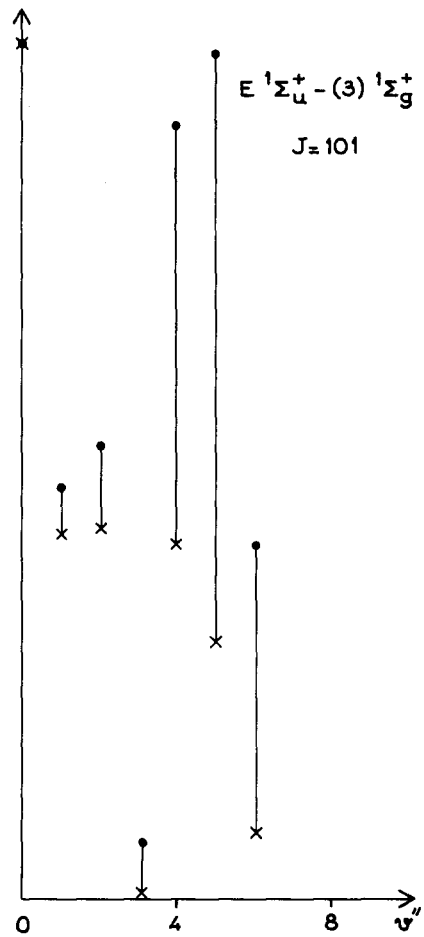

FIG. 22. Comparison between observed line intensities ($\times$) and calculated Franck–Condon factors (●) for the transitions $E\,^1\Sigma_u^+$ ($v' = 2, J' = 101$) $\rightarrow (3)\,^1\Sigma_g^+$ ($v'', J'' = 100$). See footnote of Fig. 20 for normalization ($v'' = 0$).

So, the set of molecular constants and the potential energy curves should be considered as preliminary. Further measurements have recently been done to improve the spectroscopic knowledge of this electronic state.[69]

B. Dissociation limits

With the potential energy curves of Tables XI to XIV one can now determine their dissociation limits. With the electronic term difference T_e and the energy difference of the corresponding atomic states U_A, the dissociation limits D_e' and D_e'' of the potential energy curves involved are related by

$$T_e + D_e' - D_e'' = U_A.$$

The following values (in cm^{-1}) for the atomic energy levels of cesium have been measured by means of Fourier spectroscopy[70] with an absolute accuracy of 0.02 cm^{-1}:

$6p$	$^2P_{1/2}$	11 178.27,
$6p$	$^2P_{3/2}$	11 732.31,
$5d$	$^2D_{3/2}$	14 499.26,
$5d$	$^2D_{5/2}$	14 596.85,
$7s$	$^2S_{1/2}$	18 535.53,
$7p$	$^2P_{1/2}$	21 765.35,
$7p$	$^2P_{3/2}$	21 946.40.

TABLE XV. Energies of the dissociation products relative to bottom of the $X\,^1\Sigma_g^+$ ground state.

Dissociation products	Energy (in cm^{-1})
$6s\,^2S_{1/2} + 6s\,^2S_{1/2}$	3 649.5
$6s\,^2S_{1/2} + 6p\,^2P_{1/2}$	14 827.8
$6s\,^2S_{1/2} + 6p\,^2P_{3/2}$	15 381.8
$6s\,^2S_{1/2} + 5d\,^2D_{3/2}$	18 149.0
$6s\,^2S_{1/2} + 5d\,^2D_{5/2}$	18 246.3
$6s\,^2S_{1/2} + 7s\,^2S_{1/2}$	22 185.0
$6s\,^2S_{1/2} + 7p\,^2P_{1/2}$	25 415.0
$6s\,^2S_{1/2} + 7p\,^2P_{3/2}$	25 595.9

The difference with respect to the reported values in the classical book of Moore[71] may approach more than 0.3 cm^{-1}. After their accurate study of the ground state potential energy curve considering all possible sources of errors Weickenmeier *et al.*[43] reported as their best value of D_e'' for the ground $X\,^1\Sigma_g^+$ state

$$D_e'' = 3649.5 \pm 0.8 \text{ cm}^{-1}.$$

The energies of the first dissociation products of Cs_2 are given in Table XV.

We now consider the electronic states in increasing order of the energy. It is well known from the studies of Movre and Pichler[51] and Bussery *et al.*[52] that the $(2)\,^1\Sigma_g^+$ state correlates with the $^2S_{1/2} + {}^2P_{1/2}$ atomic limit through a barrier. The dissociation energy, without the potential barrier, is then

$$D_e[(2)\,^1\Sigma_g^+] = 14\,827.8 - T_e[(2)\,^1\Sigma_g^+].$$

From Table III $T_e[(2)\,^1\Sigma_g^+] = 12\,114.07$ and

$$D_e[(2)\,^1\Sigma_g^+] = 2713.7 \pm 0.8 \text{ cm}^{-1}.$$

The second observed electronic state is the $(1)\,^1\Pi_g^+$ state which correlates with the $^2S_{1/2} + {}^2P_{3/2}$ atomic limit. The value of T_e, obtained from Table III leads to the following $D_e[(1)\,^1\Pi_g]$ value:

$$D_e[(1)\,^1\Pi_g] = 15\,381.8 - 13\,913.42,$$

$$D_e[(1)\,^1\Pi_g] = 1468.4 \pm 0.8 \text{ cm}^{-1}.$$

A satisfactory explanation of their photolysis experiment lead Collins *et al.*[37] to correlate the $(2)C\,^1\Pi_u$ and $(2)D\,^1\Sigma_u^+$ electronic states with the $^2S_{1/2} + 5d\,^2D_{5/2}$ atomic limit. The following dissociation limit is obtained:

$$D_e[(2)C\,^1\Pi_u] = 18\,246.3 - 14\,596.8,$$

$$D_e = 2297.7 \pm 0.8 \text{ cm}^{-1}.$$

The value is in reasonable agreement with the value previously reported by Raab *et al.*,[26] i.e., $2300 \pm 20\ cm^{-1}$ but of course much more accurate since the $D_e(X\,^1\Sigma_g)$ is by far better known.

Many predissociating and perturbed levels were found in the $D\,^1\Sigma_u^+$ state. As indicated above, the T_e value for this state is not very accurate and only an estimate of D_e can therefore be given:

$$D_e(D\,^1\Sigma_u^+) = 18\,246.3 - 16\,699.77,$$

$$D_e(D\,^1\Sigma_u^+) = 1546 \text{ cm}^{-1}.$$

The $(3)\,^1\Sigma_g^+$ electronic state has $T_e = 15\,975.35\ cm^{-1}$, it is highly unlikely that it dissociates into the $6s\,^2S_{1/2} + 7s\,^2S_{1/2}$ atomic limit which would give a D_e for this state in excess of 6000 cm^{-1}. The dissociation products are most likely $^2S_{1/2} + 2D$. However, there is no means to select the correct one of the two spin–orbit components of the ^2D level. The dissociation limit is then either

$$D_e = 2173 \pm 0.8 \text{ cm}^{-1} \quad \text{for the } 5d\,^2D_{3/2} \text{ limit}$$

or

$$D_e = 2271 \pm 0.8 \text{ cm}^{-1} \quad \text{for the } 5d\,^2D_{5/2} \text{ limit.}$$

It is worth noting that the $(3)\,^1\Sigma_g^+$ state has been observed in Li_2 by Bernheim *et al.*[72] and its potential energy curve have accurately been calculated by Schmidt-Mink *et al.*[73] and Konowalow *et al.*[74] This state is a shelf state due to the ion pair character over a relatively wide range of internuclear separations.[75]

The higher state studied in this work is the $(3)\,^1\Sigma_u^+$ state. There is some ambiguity about the notation ascribed to this state. Classically it is termed E state although this notation is used for two neighboring states: the $(3)\,^1\Sigma_u$ and a higher $^1\Pi_u$ state. (Noted $E'\,^1\Pi_u$ below.) Another problem comes from the fact that the E notation in Li_2 has been given to the $(3)\,^1\Sigma_g^+$ state.[73] From the T_e value of the state equal to 20 195.32 cm^{-1} and the values of the dissociation products, reported in Table XV, the state is surely correlated with the $6s\,^2S_{1/2} + 7s\,^2S_{1/2}$ atomic limit. This is corroborated by the shallow shape of the potential curve shown in Fig. 19. In Li_2 the $(3)\,^1\Sigma_u^+$ state with its shelf follows the $Li^+(^1S) + Li^-(^3P)$ ion pair curve at intermediate internuclear separations.

From the energy of the atomic limit $6s\,^2S_{1/2} + 7s\,^2S_{1/2}$ equal to 22 185.0 cm^{-1} one obtains a dissociation limit

$$D_e[(3)\,^1\Sigma_u^+] = 1989.7 \pm 0.8 \text{ cm}^{-1}.$$

C. The Λ doubling in the Π states

In Van Vleck's pure precession hypothesis[76] and in a unique perturber approximation[77] the Λ-doubling parameter q is given by

$$q = \frac{2B^2 l(l+1)}{E_\pi - E_\Sigma},$$

where B is the rotational constant of the $^1\Pi$ state and $l(l+1)$ is the square angular momentum of the electron in the atomic state into which both molecular states dissociate.

We first consider the $(1)\,^1\Pi_g$ electronic state. The only Σ_g^+ state belonging to the same complex[77] or to the same states $^2S_{1/2} + {}^2P$ of the separated atoms is the $(2)\,^1\Sigma_g^+$ state. If we assume that $E_\Pi - E_\Sigma$ is given by the difference of the corresponding electronic term energies

$$T_e[(1)\,^1\Pi_g] - T_e[(2)\,^1\Sigma_g^+] = 13\,913.42 - 12\,114.07 = 1799.35 \text{ cm}^{-1}.$$

With B taken to be the Y_{01} coefficient (Table IV) and $l = 1$, one obtains $q = 1.35 \times 10^{-7}\ cm^{-1}$ which is to be compared with the y_{01} parameter of $2.1 \times 10^{-7}\ cm^{-1}$. The agreement is not very good and the assumed approximations seem inadequate to derive an accurate value for the Λ-doubling parameter.

The Λ doubling in the $^1\Pi_u$ state was also studied by Raab *et al.*[26] assuming a pure perturber approximation to be valid between the $C\,^1\Pi_u$ and $D\,^1\Sigma_u^+$ states. In this case the observed and the calculated parameters disagree by a factor of 3, due to the very different potential energy curves of the two states, particularly of their internuclear distances.

In fact the Van Vleck's pure precession approximation of the Λ doubling requires many approximations[68]:

unique perturber,

identical potential curves,

the two interacting states are each described by a single configuration. For the two states the configurations are identical except for a single spin–orbital which is a pure atomic one.

Clearly a more refined theoretical treatment is needed in order to explain our "experimental" Λ-doubling constants. These calculations will be presented in a forthcoming paper.

VI. SUMMARY

A comprehensive analysis of several systems of the Cs_2 molecule was made using the experimental techniques of polarization spectroscopy, double resonance, laser induced fluorescence studied by Fourier transform spectroscopy. Incorporating more than 8000 lines, the currently most accurate set of molecular constants for the five electronic states has been obtained through a global least-squares fit of all presently available high resolution spectroscopic data. The IPA potential energy curves and dissociation energies have been accurately determined for all these electronic states.

ACKNOWLEDGMENTS

C. Amiot is greatly indebted to Dr. J. Verges for the high quality Fourier spectra he has recorded on his Fourier interferometer. C. Crepin is acknowledged for his help in the assignment of some Fourier spectra. C. Amiot thanks the Laboratoire de Physique Moléculaire and Optique Atmosphérique for his financial support in the earlier stages of this work. All computer calculations were done at C.I.R.C.E. (ORSAY).

[1]F. W. Loomis and P. Kusch, Phys. Rev. **46**, 292 (1934).
[2]P. Kusch and M. M. Hessel, J. Mol. Spectrosc. **25**, 205 (1968).
[3]P. Kusch and M. M. Hessel, J. Mol. Spectrosc. **32**, 181 (1969).
[4]M. Lapp and L. P. Harris, J. Quant. Spectrosc. Radiat. Transfer **6**, 169 (1966).
[5]R. Gupta, W. Happer, J. Wagner, and E. Wennmyr, J. Chem. Phys. **68**, 799 (1978).
[6]J. Tellinghuisen and M. B. Moeller, Chem. Phys. **50**, 301 (1980).
[7]R. P. Benedict, D. L. Drummond, and L. A. Schlie, J. Chem. Phys. **66**, 4600 (1977).
[8]D. S. Bayley, E. C. Eberlin, and J. H. Simpson, J. Chem. Phys. **49**, 2863 (1968).
[9]N. N. Kostin and V. A. Khodovoi, Izv. Akad. Nauk USSR Ser. Fiz. **37**, 2093 (1973).
[10]E. Zouboulis, N. D. Bhaskar, A. Vasilakis, and W. Happer, J. Chem. Phys. **72**, 2356 (1980).
[11]D. M. Creek and G. V. Marr, J. Quant. Spectrosc. Radiat. Transfer **8**, 1431 (1968).
[12]R. Hotop and K. Niemax, J. Phys. B **13**, L93 (1980).
[13]R. P. Benedict, D. L. Drummond, and L. A. Schlie, J. Chem. Phys. **70**, 3155 (1979).
[14]M. McClintock and L. C. Balling, J. Quant. Spectrosc. Radiat. Transfer **9**, 1209 (1969).
[15]G. York and A. Gallagher, JILA Report No. 144, University of Colorado, Boulder, Colorado (1974).
[16]M. M. Hessel and C. R. Vidal, J. Chem. Phys. **70**, 4439 (1979).
[17]K. K. Verma, J. T. Banhs, A. R. Rajaei-Rizi, W. C. Stwalley, and W. T. Zemke, J. Chem. Phys. **78**, 3599 (1983).
[18]H. Helling and B. Wellegehausen, in *Laser Spectroscopy III*, edited by J. L. Hall and J. L. Carlsten (Springer, Berlin, 1977), p. 365.
[19]M. A. Henesian, R. L.Herbst, and P. L. Byer, J. Appl. Phys. **47**, 1515 (1976).
[20]H. Itoh, H. Uchiki, and M. Matsuoko, Opt. Commun. **18**, 271 (1971).
[21]B. Wellegehausen, S. Shahdin, D. Friede, and H. Welling, Appl. Phys. **13**, 97 (1977).
[22]H. Katô and K. Yoshihara, J. Chem. Phys. **71**, 1585 (1979).
[23]G. Höning, M. Cazjkowski, M. Stock, and W. Demtröder, J. Chem. Phys. **71**, 2138 (1979).
[24]A. I. Kobyliansky, A. N. Kulikov, and L. V. Gurvich, Chem. Phys. Lett. **62**, 198 (1979).
[25]M. Raab, G. Höning, R. Castell, and W. Demtröder, Chem. Phys. Lett. **66**, 307 (1979).
[26]M. Raab, G. Höning, W. Demtröder, and C. R. Vidal, J. Chem. Phys. **76**, 4370 (1982).
[27]N. D. Bhaskar, E. Zouboulis, R. Novak, and W. Happer, Chem. Phys. Lett. **63**, 555 (1979).
[28]Z. Wu, M. Ligare, and W. Happer, Phys. Lett. A **89**, 7 (1982).
[29]C. Amiot, C. Crepin, and J. Verges, Chem. Phys. Lett. **98**, 608 (1983).
[30]C. Amiot, C. Crepin, and J. Verges, J. Mol. Spectrosc. **107**, 28 (1984).
[31]C. Amiot, C. Crepin, and J. Verges, Chem. Phys. Lett. **106**, 162 (1984).
[32]C. Amiot and J. Verges, Chem. Phys. Lett. **116**, 273 (1985).
[33]C. B. Collins, B. W. Johnson, M. Y. Mirza, D. Popescu, and I. Popescu, Phys. Rev. A **10**, 813 (1974).
[34]E. H. A. Granneman, M. Klewer, K. J. Nygaard, and M. J. Van der Wiel, J. Phys. B **9**, 865 (1976).
[35]C. B. Collins, J. A. Anderson, F. W. Lee, P. A. Vicharelli, D. Popescu, and I. Popescu, Phys. Rev. Lett. **44**, 139 (1980).
[36]C. B. Collins, J.A. Anderson, D. Popescu, and I. Popescu, J. Chem. Phys. **74**, 1053 (1981).
[37]C. B. Collins, F. W. Lee, J. A. Anderson, P. A. Vicharelli, D. Popescu, and I. Popescu, J. Chem. Phys. **74**, 1067 (1981).
[38]G. Baumgartner, W. Demtröder, and M. Stock, Z. Phys. **232**, 462 (1970).
[39]Z. Wu and J. Huennekens, J. Chem. Phys. **81**, 4433 (1984).
[40]H. Katô and K. Onomichi, J. Chem. Phys. **82**, 1642 (1985).
[41]M. Raab, H. Weickenmeier, and W. Demtröder, Chem. Phys. Lett. **88**, 377 (1982).
[42]R. J. Le Roy, *Molecular Spectroscopy*, Chemical Society Specialist Periodical Report (The Chemical Society, London, 1973), Vol. 1, pp. 113–176. R. J. Le Roy and R. B. Bernstein, J. Chem. Phys. **52**, 3869 (1970).
[43]H. Weickenmeier, U. Diemer, M. Wahl, M. Raab, W. Demtröder, and W. Müller, J. Chem. Phys. **82**, 5354 (1985).
[44]H. Weickenmeier, U. Diemer, W. Demtröder, and M. Broyer, Chem. Phys. Lett. **124**, 470 (1986).
[45]B. C. Laskowski and St. R. Langhoff, Chem. Phys. Lett. **92**, 49 (1982).
[46]St P. Walch, Ch. W. Bauschlicher Jr., P. E. M. Siegbahn, and H. Partridge, Chem. Phys. Lett. **92**, 54 (1982).
[47]G. H. Jeung, F. Spiegelmann, J. P. Daudey, and J. P. Malrieu, J. Phys. B **16**, 2659 (1983).
[48]A. Dalgarno, Adv. Chem. Phys. **12**, 143 (1967).
[49]K. T. Tang, J. M. Norbeck, and P. R. Certain, J. Chem. Phys. **64**, 3063 (1976).
[50]F. Vigne-Mader, Chem. Phys. **85**, 139 (1984).
[51]M. Movre and G. Pichler, J. Phys. B **10**, 2631 (1977).
[52]B. Bussery and M. Aubert-Frecon, J. Chem. Phys. **82**, 3224 (1985).
[53]H. P. Layer, R. Deslattes, and W. G. Schweitzer, Appl. Opt. **15**, 734 (1976).
[54]P. Jacquinot, J. Phys. (Paris) **19**, 223 (1958).
[55]P. Fellgett, J. Phys. (Paris) **19**, 187 (1958).
[56]J. Connes, H. Delouis, P. Connes, G. Guelachvili, J. P. Maillard, and G. Michel, Nouv. Rev. Opt. Appl. **1**, 3 (1970).
[57]C. Crepin, Thèse de 3ème cycle, Université Paris XI, France, 1984.
[58]C. R. Vidal and J. Cooper, J. Appl. Phys. **40**, 3370 (1969).
[59]W. Demtröder, *Laser Spectroscopy* (Springer, Heidelberg, 1982).

[60]A. N. Nesmeyanov, *Vapor Pressure of the Chemical Elements* (Elsevier, New York, 1963).
[61]G. Herzberg, *Molecular Spectra and Molecular Structure*, 2nd ed. (Van Nostrand, Princeton, 1950).
[62]J. L. Dunham, Phys. Rev. **41**, 721 (1932).
[63]D. L. Albritton, A. L. Schmeltekopf, and R. N. Sare, in *Molecular Spectroscopy: Modern Research*, edited by K. Narahari Rao (Academic, New York, 1976), Vol. II.
[64]W. M. Kosman and J. Hinze, J. Mol. Spectrosc. **56**, 93 (1975).
[65]C. R. Vidal and H. Scheingraber, J. Mol. Spectrosc. **65**, 46 (1977).
[66]C. R. Vidal, Comments At. Mol. Phys. **17**, 173 (1986).
[67]R. Rydberg, Z. Phys. **73**, 376 (1931); **80**, 514 (1933); O. Klein, *ibid.* **76**, 226 (1932); A. L. G. Rees, Proc. Phys. Soc. London **59**, 998 (1974).
[68]H. Lefebvre-Brion and R. W. Field, *Perturbations in the Spectra of Diatomic Molecules* (Academic, New York, 1986), p. 190.
[69]U. Diemer, J. Keto, W. Weickenmeier, and W. Demtröder, J. Chem. Phys. (to be published).
[70]J. Verges (private communication, unpublished).
[71]C. E. Moore, *Atomic Energy Levels*, Natl. Stand. Ref. Data Ser. Natl. Bur. Stand. 35 (U. S. GPO, Washington, D.C., 1971).
[72]R. A. Bernheim, L. P. Gold, P. B. Kelly, T. Tipton, and D. K. Veirs, J. Chem. Phys. **76**, 57 (1982).
[73]I. Schmidt-Mink, W. Müller, and W. Meyer, Chem. Phys. **92**, 263 (1985).
[74]D. D. Konowalow and J. L. Fish, Chem. Phys. **84**, 463 (1984).
[75]R. A. Bernheim, L. P. Gold, C. A. Tomczyk, and C. R. Vidal, J. Chem. Phys. **87**, 861 (1987).
[76]J. H. Van Vleck, Phys. Rev. **33**, 467 (1929).
[77]R. S. Mulliken and A. Christy, Phys. Rev. **38**, 87 (1931).
[78]J.T. Hougen, Natl. Bur. Stand. (U.S.) Monogr. 115 (1970).